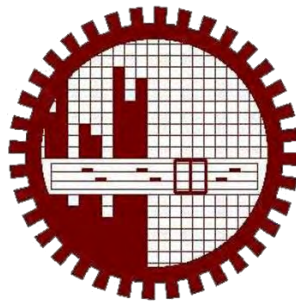


SYNTHESIS AND PERFORMANCE EVALUATION OF BIOCHAR/CHITOSAN/ZnO COMPOSITE FOR DYE REMOVAL FROM AQUEOUS SOLUTION

MOHAMMAD TANVIR ARIFIN

A thesis submitted to the Department of Chemical Engineering in partial
fulfillment of the requirements for the degree of
MASTER OF SCIENCE IN ENGINEERING (CHEMICAL)



DEPARTMENT OF CHEMICAL ENGINEERING
BANGLADESH UNIVERSITY OF ENGINEERING &
TECHNOLOGY (BUET)
DHAKA, BANGLADESH

APRIL 2022

CANDIDATE'S DECLARATION

I do hereby, declare that this thesis paper or any part of it has not been submitted elsewhere for the award of any other degree or diploma.

Tanvir Arifin

Mohammad Tanvir Arifin

Date: 23 April 2022

CERTIFICATION OF THESIS WORK

We the undersigned, glad to certify that **Mohammad Tanvir Arifin**, candidate for the degree of Master of Science in Engineering (Chemical) has presented his thesis work title “**Synthesis and Performance Evaluation of Biochar/Chitosan/ZnO Composite for Dye Removal from Aqueous Solution**”. The thesis is acceptable in form and content. The student demonstrated satisfactory knowledge of the field covered by this thesis in an oral examination held on April 23, 2022.



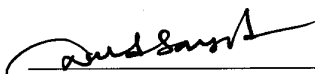
Dr. Md. Shahinoor Islam
Professor
Department of Chemical Engineering
BUET, Dhaka-1000.

**Chairman
(Supervisor)**



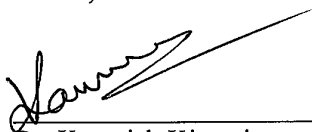
Dr. Md. Mominur Rahman
Professor and Head
Department of Chemical Engineering
BUET, Dhaka-1000.

**Member
(Ex-Officio)**



Dr. Nahid Sanzida
Associate Professor
Department of Chemical Engineering
BUET, Dhaka-1000.

Member



Dr. Kawnish Kirtania
Associate Professor
Department of Chemical Engineering
BUET, Dhaka-1000.

Member



Dr. Md. Nazrul Islam
Professor
Department of Chemistry
BUET, Dhaka-1000.

**Member
(External)**

*To my parents and elder brother,
who inspired me to accomplish this purpose*

ACKNOWLEDGEMENT

All praise is due to Allah alone, because of the strength and purposefulness that He gave me to fulfill this goal.

I would like to express my deepest appreciation to my thesis supervisor **Dr. Md. Shahinoor Islam** who conveyed a spirit of adventure regarding research. Without his guidance and continuous assistance, this dissertation would not have been possible. I sincerely appreciate the knowledge he has shared with me and the opportunities he has given me to grow as a researcher. It is a blessing to find a mentor who has not only taught me how to be more inquisitive but also more patient when it came to research because scientific investigation is never a smooth-sailing endeavor.

I would like to thank **Dr. Md. Shakhawat Hossain Firoz**, Professor who has been integral to this project from the very beginning, for providing his valuable insight about nano-composites so that I could bring this project to fruition and facilities to carry out my research work in his laboratory. Without the constant support and guidance from Professor **Dr. Md. Shahinoor Islam** and **Dr. Md. Shakhawat Hossain Firoz**, this thesis work would not be successful.

The Atomic Energy Research Center at Savar has been instrumental in supporting a significant portion of the project, by carrying out the characterization of the bio-adsorbent materials. I express my sincere gratitude to the people at the AERC.

Finally, I would also like to thank and be grateful to my lab mates, **Hridoy Roy** and **Ehsanur Rahman** for assisting me in the project and working with sincerity and diligence. I wish them even greater success in their own future research endeavors.

ABSTRACT

Textile effluents have become a major concern to environmentalists due to the bio-persistent nature of the dyes. The azo dyes are toxic to human and aquatic life. In recent years, treatment of contaminated effluents by natural resources has been proposed as the most sustainable solution for this problem. In this work, *Moringa oleifera* seeds derived biochar in combination with chitosan and ZnO were used to produce three binary composites such as Biochar-Chitosan (BC), Biochar-ZnO (BZ), and Chitosan-ZnO(CZ) along with a ternary composite Chitosan-ZnO/Biochar (CZB). The prepared composites were characterized by Fourier Transform-Infrared Spectroscopy (FTIR), Field Emission Scanning Electron Microscope (SEM), and X-ray diffraction (XRD). The surface area of the prepared materials was measured by the Brunauer-Emmett-Teller (BET) analyzer. The adsorption efficiency of these composites was evaluated against a cationic azo dye, methylene blue (MB). Spectroscopic analysis of the biochar-based composites established that the modification of biochar by chitosan and ZnO enhanced different functional groups e.g., -OH, -COOH, R-CH, R-OH, -NH₂, etc., and active groups on the biochar surface. The presence of micro and mesopores in the structure of biochar is revealed by FESEM images. Pore development of biochar by ZnO particles was also visible. The XRD results showed the highly amorphous structure and increased crystallinity of biochar by the modification. The surface area ranged from 0.90 ± 0.00 to $14.48 \pm 1.13 \text{ m}^2\text{g}^{-1}$ for prepared samples, where the highest surface area was found for BZ and the lowest for BC. Basic pH was found to be favorable for adsorption. Rapid dye adsorption was observed in the time range of 0-20 min, reaching its saturation at 90 min. The impact of dye concentration dependence was evaluated in the range of 10-70 mgL^{-1} . The kinetics data were linearized by two different kinetics models e.g., pseudo 1st order and pseudo 2nd order model. Isotherm reveals the favorability of Langmuir isotherm over the Freundlich and Tempkin models. The highest adsorption capacity was found for BC followed by the second-highest for CZB. For the binary composite BC and ternary composite CZB, the RSM optimizations were also conducted, which gave similar results that were observed in the experiments. The characterization and experimental results prefigure the chemical functionalities were the critical parameters over the surface area for the adsorption process.

TABLE OF CONTENTS

ABSTRACT	i
ACKNOWLEDGMENT	ii
LIST OF FIGURES	vi
LIST OF TABLES	vii
LIST OF ABBREVIATIONS AND SYMBOLS	viii ix
CHAPTER 1	
INTRODUCTION	1
1.1 Background	2
1.2 Significance of the Study	4
1.3 Objectives of the Study	4
1.4 Thesis Outline	5
CHAPTER 2	
LITERATURE REVIEW	6
2.1 Adsorption process	7
2.1.1 Natural Adsorbents	7
2.1.2 Biomass-based adsorbents	8
2.1.3 <i>Moringa oleifera</i> -derived adsorbents	9
2.1.4 Modified biomass-based adsorbents	11
2.2 Factors affecting Adsorption of Dye	12
2.2.1 Effect of Solution pH	12
2.2.2 Effect of Initial Dye Concentration	12
2.2.3 Effect of Temperature	12
2.2.4 Effect of Amount of Adsorbents	13
2.3 Selection of Synthetic Dye	13

2.3.1	Azo dye	14
2.3.2	Methylene Blue	14
2.4	Adsorbents Characterization and Analytical Techniques	15
2.4.1	Fourier Transform Infrared Spectroscopy (FTIR)	15
2.4.2	X-ray Diffraction (XRD)	15
2.4.3	Nitrogen Physisorption Measurement (BET analysis)	16
2.4.4	UV-Vis- NIR Spectrophotometer	16
2.4.5	Scanning Electron Microscope (SEM)	16
CHAPTER 3		
METHODOLOGY		
		17
3.1	Materials	18
3.2	Experimental Design	18
3.2.1	Biochar (B) preparation	18
3.2.2	Biochar/Chitosan (BC) preparation	19
3.2.3	Biochar/ZnO (BZ) preparation	19
3.2.4	Chitosan/Zinc Oxide (CZ) preparation	19
3.2.5	Chiosan/ZnO/Biochar (CZB) preparation	19
3.3	Characterization of adsorbents	20
3.4	Experimental Design	20
3.5	Statistical Design	21
3.6	Isotherms and Kinetics Modeling	22
3.6.1	Isotherms	22
3.6.1.1	Langmuir isotherm model	22
3.6.1.2	Freundlich isotherm model	23
3.6.1.3	Temkin isotherm model	24
3.6.2	Adsorption Kinetics	25
3.6.2.1	Pseudo-first-order adsorption kinetics	25
3.6.2.2	Pseudo-second-order adsorption kinetics	25

CHAPTER 4	
RESULTS & DISCUSSION	26
4.1 Characterization of Synthesized Materials	27
4.2 Impact of pH and dye concentration on adsorption	34
4.3 Effect of Contact Time and Adsorption Kinetics	35
4.4 Effect of Initial Concentration and Adsorption Isotherms	37
4.5 Response Surface Analysis for CZB	43
4.5.1 Effect of Independent Variables on Response Variable (removal%)	43
4.5.2 Optimization of independent variables and verification of RSM model	44
4.6 Response Surface Analysis for BC	45
4.6.1 The model fitting	45
4.6.2 Effect of independent variables on a response variable(removal%)	48
4.7 Adsorption Mechanism	50
CHAPTER 5	52
CONCLUSION AND FUTURE WORK	
5.1 Conclusion	53
5.2 Future Work	54
REFERENCES	55

LIST OF FIGURES

Fig. 1. Structure of Methylene Blue	14
Fig. 2. Comparison of the FTIR spectra of Biochar (a), CZ (b) and CZB	28
Fig. 3. XRD images of biochar, CZ and CZB	28
Fig. 4. Scanning electron microscope (SEM) micrograph (left) and energy-dispersive X-ray spectroscopy (EDS) spectra (right) of biochar (a), CZ (b), and CZB (c)	30
Fig. 5. Energy-dispersive X-ray spectroscopy (EDS) spectra of biochar (a), BC (b), BZ (c), CZ (d), and CZB (e)	32
Fig. 6. Effect of pH on adsorption of MB by Biochar (black), Chitosan (purple), ZnO (light purple), BC(red), BZ (orange), CZ(blue), and CZB (green)	35
Fig. 7. Effect of time on adsorption of MB by Biochar (black), Chitosan (purple), ZnO (light purple), BC(red), BZ (orange), CZ(blue), and CZB (green)	36
Figure. 8. Linear fittings of pseudo-first (a) and pseudo-second (b) order kinetics.	37
Fig. 9. Effect of concentration on adsorption of MB by Biochar (black), Chitosan (purple), ZnO (light purple), BC (red), BZ (orange), CZ (blue), and CZB (green)	38
Fig. 10. Combined effects of pH and time (a), concentration and time (b) pH and concentration (c) on removal (%)	43
Fig. 11. Combined effects of pH and time (a), concentration and time (b) pH and concentration (c) on removal (%) for BC	49

LIST OF TABLES

Table 1. Different feedstocks, pyrolysis temperature, and potentials applications of biochar	8
Table 2. Different preparation methods and performances of <i>M. oleifera</i> -derived adsorbents	10
Table 3. Independent variables and their corresponding levels for removal (%).	21
Table 4. Significance of slope 1/n	24
Table 5. Elemental composition of prepared samples from Energy-dispersive X-ray spectroscopy (EDS)	32
Table 6. BET surface area of biochar, BC, BZ, CZ and CZB. BC stands for Biochar-chitosan, BZ stands for Biochar-ZnO, CZ stands for chitosan-ZnO and CZB stands for chitosan-ZnO/biochar.	32
Table 7. The average particle size of biochar, BC, BZ, CZ, and CZB from SEM image by ImageJ software	33
Table 8. Kinetics modeling parameters obtained for pseudo-1 st order, pseudo-2 nd order model. BC stands for Biochar-chitosan, BZ stands for Biochar-ZnO, CZ stands for chitosan-ZnO and CZB stands for chitosan-ZnO/biochar.	36
Table 9. Isotherm modeling parameters were obtained for Langmuir, Freundlich, and Temkin Isotherms. BC stands for Biochar-chitosan, BZ stands for Biochar-ZnO, CZ stands for chitosan-ZnO and CZB stands for chitosan-ZnO/biochar.	39
Table 10. The ANOVA analysis of the quadratic polynomial model with a coefficient of determination (R^2) value of 0.9843 for removal (%).	40
Table 11. The ANOVA analysis of the variance quadratic model for removal of the dye	41
Table 12. Regression coefficient values for removal (%).	42
Table 13. Optimum conditions and removal (%) at optimized condition	45
Table 14. Independent parameters and their corresponding levels for percentage removal (% R) for BC	46
Table 15. The ANOVA analysis of the variance quadratic model for removal of the dye	47

LIST OF ABBREVIATIONS AND SYMBOLS ABBREVIATIONS

BC	Biochar-Chitosan
BZ	Biochar-Zinc Oxide
CZ	Chitosan-Zinc Oxide
BET	Brunauer-Emmett-Teller
XRD	X-ray diffraction
FESEM	Field emission scanning electron microscope
RSM	Response Surface Methodology
FTIR	Fourier transform infrared spectroscopic
MB	Methylene Blue
AC	Activated Carbon
TOC	Total Organic Carbon
COD	Chemical Oxygen Demand
BOD	Biological Oxygen Demand
CZB	Chitosan Zinc Oxide-Biochar
CCD	Central composite design
EDS	Energy-dispersive X-ray spectroscopy
SEM	Scanning electron microscope

SYMBOLS

-OH	Hydroxyl group
-COOH	Carboxyl group
R-CH ₃	Methyl group
R-OH	Alcohol group
CH ₃ COOH	Acetic Acid
-NH ₂	Amino radical
ZnO	Zinc-Oxide
λ_{\max}	lambda
B	Beta
Π	pi
R _L	Separation factor
K _L	Langmuir isotherm constant
K _F	Freundlich isotherm constant
Q _e	adsorption capacity
C _e	dye concentration

CHAPTER **1**

INTRODUCTION

1.1 Background

Water pollution is a great concern nowadays. Increasing water demand to different chemical industries e.g., textile, pharmaceuticals, oil field, cosmetics, paper, food, etc., results in higher effluent volumes which are discharged into the environment with little or no treatment at all (Al-Mamun et al., 2019; Baptisttella et al., 2021; Islam et al., 2015; Pereira et al., 2013; Pourrezaei et al., 2010; Roy et al., 2022). As a result, water is polluted severely, and reaching of a scarcity of safe water in the community (Akter et al., 2022; Rashid et al., 2021a; Suhan et al., 2021). Besides, toxic chemicals are applied for agricultural and industrial purposes, and the untreated leftover toxic chemicals leach into the groundwater causing groundwater pollution (Foster 2017; Hwang et al., 2013; Islam et al., 2014a; Shafiq et al., 2019). As a result of the contamination of groundwater, we are going to deprive of this natural gift and are forced to adapt to a big challenge and the depletion of aquifers has been observed recently (Kannaujiya et al., 2019). The major sources of water pollution are municipal waste, industrial waste, pesticides, pharmaceutical waste, and fertilizer waste from agriculture (Akter et al., 2022; Crini and Lichtfouse 2019; Islam et al., 2012; Islam et al., 2014b). The major contaminants in wastewater effluents are hydrogenated hydrocarbons, pesticides, herbicides, heavy metals, used lube oil, dyes, surfactants, nutrients (mainly nitrogen and phosphorous) organic compounds, acids, salts, bases, etc. (Chauhan et al., 2019; Islam et al., 2021; Kwak et al., 2019; Islam et al., 2017; Saravanan et al. 2019). Among industrial wastes, textile, paper, and food industries tend to generate the largest amount of industrial wastewater according to recent studies. Mainly, synthetic dyes are widely discharged into water bodies as major contaminants from these industries and contribute significantly to water pollution (Roy et al., 2022; Yusuf et al., 2019; Ismail et al., 2019). The dye's complex structures, synthetic origin, and recalcitrant nature are characteristics that make it harmful to the environment (Shah et al., 2013). Wastewater containing dyes is considered highly toxic for humans (Choi et al., 2013; Sahnoun et al., 2018) and alters water chemistry by changing the pH, oxygen level, color, and organic content of the water bodies, as well as inhibiting the growth of microbial organisms (Akter and Islam, 2022; Chenlu et al., 2020; Zhang et al., 2017). The efficient removal of dyes from effluents is a big challenge because of its toxic and persistent nature. Existing technologies include biological treatment methods, coagulation, photo-Fenton processes, ozonation, oxidation, filtration, activated carbon adsorption, and reverse osmosis (Yang et al., 2020; Yogalakshmi et al., 2020). However, some of these methods are not practical from an economic and environmental

point of view. In some processes, an undesirable quantity of waste or residue is generated, which makes the process complicated and time-consuming. As a result, it is critical to investigate alternative and appropriate technologies for the removal of toxic dyes. However, there is a growing interest in using low-cost, readily available materials for the adsorption of dyes. The adsorption process for water treatment has received a lot of attention as it offers low energy consumption, high efficiency, and ease of operation (Samsami et al., 2020; Gwenzi et al., 2017; Kwak et al., 2019). In addition, a large volume of wastewater can be treated with no harmful residue (Dutta et al., 2021; Saxena et al., 2020). In recent years, different adsorbents have already been reported e.g., alumina (Banerjee et al., 2019), zeolites, bentonite clays, graphene oxide (GO), activated-carbon (AC) (Herrera-González et al., 2019) biochar (Sackey et al., 2021), etc. However, excluding activated carbon and biochar, the rest of the adsorbents are reported to be very efficient for dye removal from aqueous solution but have some major drawbacks with initial cost, unavailability of raw materials, and complicated synthesis process (Ikram et al., 2020; Smith et al., 2021). For large-scale operation, AC and biochar are found to be very efficient, in which AC preparation requires some sequential steps e.g., carbonization, physical, and chemical activations; whereas biochar preparation is very simple and effective (Pan et al., 2021; Patawat et al., 2020; Yaashika et al., 2020). In recent years, biochar-based adsorbents have been reported as impressive adsorbents for various dye contaminants. The adsorptive properties are attributed to (1) its surface area, which confirms adsorption sites for dye molecules; and most importantly (2) the presence of several functional groups on the surface, which can form complexes with different types of dyes. The adsorption properties of the biochar are directly affected by its parent source. An appropriate biomass source that is readily available is a critical requirement for selecting an adequate parent source for biochar production. Different bio-sources e.g., sawdust, canola straw, rice straw, rice husk, citrus peel, peanut shell, pine wood, etc. are used to produce biochar. The adsorption capacities and interaction mechanisms of biochar with dye pollutants mainly depend on dye properties/ion charges, biochar chemical composition, biochar properties, modification/activation, the aging process, and environmental conditions. However, immaculate biochar hardly exhibits high adsorption efficiency for capturing toxic organic pollutants and suffers from a lack of selectivity (Zhao et al., 2020). To overcome these constraints, emphasis has further been focused on the modification of biochar by different polymers e.g., cellulose, pectins, chitosan, and metal oxides e.g., CaO, CuO, ZnO (Wang et al., 2019). Therefore, the main objective of the current

study was to synthesize three different binary composites and a tertiary composite e.g., biochar-chitosan (BC), biochar-ZnO (BZ), chitosan-ZnO (CZ), and chitosan-ZnO-biochar (CZB) to investigate the performance of the composites in the adsorption of methylene blue (MB) cationic dye. In this study, *Moringa oleifera* seed was used as the parent source of biochar that exhibited as an intriguing natural adsorbent for dye removal. *M. oleifera* is a tropical and subtropical plant with a high seed yield and ease of availability. The methylene blue dye was used for the current study because it is used as a common dye in the dyestuff industries. Moreover, the methylene blue dye is cationic in nature and created complex structures with the adsorbents during the removal of initial dye concentrations. However, it contains the $-N=N-$ group in its structure, known as an azo compound that has many negative environmental effects. It contains a fused aromatic ring that resists biodegradation. The azo group converts to toxic amines from microbial activities. These amines, as well as the existing azo group, can easily enter the human food chain and cause allergies, dermatitis, and cancer (Pea-Guzmán et al., 2019).

1.2 Significances of the Study

The entire world is currently moving toward a sustainable environmental solution, and wastewater management is a critical component of this. As a result, the proposed study's main goal was to provide an idea for a simple biochar-based textile wastewater treatment. This paper's customized biochar-based adsorbent will be able to provide knowledge on laboratory-scale research and the subsequent need to scale up for industrial application. Overall, the proposed application of biochar-based adsorbent can be regarded as one of the key strategies for the sustainable management of wastewater in terms of environmental, public health, and greener economic impacts.

1.3 Objectives of the Study

The primary goal of this project was to investigate the performance of a laboratory-created biochar/chitosan/zinc oxide-based composite material on the removal of methylene blue dye in an aqueous solution. The following were the specific goals-

- Synthesis of biochar/chitosan/ZnO as surface-modified adsorption materials using biochar and chitosan/ZnO composite
- Characterization of surface morphology and surface functional groups of ZnO, chitosan, chitosan/ZnO nanocomposite, and Biochar/chitosan/ZnO composite using FTIR, SEM, and XRD

- Investigation of adsorption behavior (using isotherm and kinetic study) for both pristine biochar, and binary composites against a cationic dye methylene blue
- Optimization of adsorption conditions by changing pH, contact time, and initial concentrations to maximize the sorption
- Statistical analysis of adsorption using response surface methodology (RSM).

1.4 Thesis Outlines

Chapter 1: This chapter provides the background, significance, and objective of the current study.

Chapter 2: Literature reviews on related works to the fundamental knowledge of dye adsorption have been provided in this chapter. It summarizes adsorption mechanisms, factors of dye removal activity, and modification of biochar-based adsorbents.

Chapter 3: This chapter summarizes all the materials required for the study, experimental methods, and procedures applied during this research. At first, the binary and ternary composites preparation techniques of *M. oleifera* biochar-based adsorbent have been described in the Chapter. Then, the Chapter presents the characterization techniques applied to the adsorbents. The final sub-section of the Chapter includes adsorption experimental setup, diagrams, and detailed experimental procedures.

Chapter 4: This chapter focuses on the observed results of the applied adsorbents to dye removal. All the adsorbent characterization results have been well presented and thoroughly discussed. The chapter includes the performance of the synthesized adsorbents for the removal of methylene blue. The factors affecting the preparation and synthesis of *M. oleifera* biochar on dye adsorption have been discussed systematically. The impact of pH on dye adsorption has been presented. Finally, the RSM methodology has been well discussed in the context of the obtained results.

Chapter 5: This chapter summarizes the outcomes of the study and concludes with achievements from the current study. It also recommends future work based on the current study.

CHAPTER 2

LITERATURE REVIEW

2.1 Adsorption Process

The adsorption process is a cost-effective and efficient method to remove pollutants from wastewater. In this process, soluble or removed species from a liquid phase to a solid phase are transported to a solid phase (Islam et al., 2014c; Anil et al., 2020). Adsorbed species are bound to the surface through physicochemical interactions (Jahan et al., 2022; Manchisi et al., 2020). Generally, three sequential steps are involved in adsorbate adsorption: (1) transport of adsorbate to the border outer space of the adsorbent; (2) diffusion through the pores; and (3) adsorption of solutes and desorption (Islam et al., 2018). During all these steps, the rate of each step is governed by the properties of adsorbates, adsorbents, and contaminant matrix. Adsorption isotherms are used to calculate the maximum adsorption capacity of a material (Islam et al., 2015c). A low-cost adsorbent is produced from naturally abundant materials such as plant and animal wastes, Mustard husk, chitosan, oil palm trunk fibers, sugarcane bagasse, and nutshell are examples of plant-based feedstocks for adsorbents (Rosales et al., 2017). Egg shells, cow dung, etc. are examples of animal waste to produce adsorbent. Therefore, in recent years, the use of natural biological adsorbents (biomaterials) derived from agricultural materials has been promoted as an alternative and cost-effective technology for pollutant removal.

2.1.1 Natural adsorbents

In particular, adsorption on activated carbons is an effective method for removing dyes from wastewater, an alternative to more expensive treatment methods. However, activated carbon has several drawbacks, including regeneration and it is non-selective and ineffective against dispersing and vat dyes. The removal of MB dye by adsorption on different ACs was found to be rapid during the initial contact time and then slow and stagnant as contact time increased. The removal of methylene blue (MB) by adsorption on the surface of ACs because of MB in its cationic form (Hasanzadeh et al., 2020). The adsorption rate and increase in contact time will affect the boundary layer resistance because dye uptake at the active sites of AC is a rapid process and the adsorption rate is primarily governed by the liquid phase mass transfer rate and the intraparticle mass transfer rate. Naturally occurring materials such as chitosan, kaolin clay, coal, sand, zeolite, peat moss, alumina, and wood have been successfully used as adsorbents to remove organics, and heavy metal, surfactants, and dyes from wastewater (Rashid et al., 2021). They are advantageous because of their economic feasibility and availability. Zeolites are naturally occurring aluminosilicate crystals structure linked together by oxygen atoms and are applied in industry for different

purposes such as adsorption of gaseous substances for the production of nitrogen and oxygen from the air (Rendo, 2021). Clay minerals are non-toxic, available, and abundant. These materials can be applied as adsorbents because the surface is negatively charged and has colloidal properties which enhance their ability to adsorb organic molecules and cations (Ayisha Sidiqia and Priya, 2021).

2.1.2 Biomass-based adsorbents

Bio-adsorbent (agriculture-based) or biochar has significant competency in metal, dyes, and organics removal from wastewater (Islam et al., 2018; Roy et al., 2022; Wang et al., 2020). Biochar is a low-cost adsorbent material produced from a variety of biomass feedstock types through pyrolysis under different temperatures and low or in the absence of oxygen conditions (Islam et al. 2021b). The production cost of biochar (\$245 ton⁻¹) is significantly lower than that of activated carbon (\$1450 ton⁻¹), which has been used as a traditional sorbent (Ahmad et al., 2012; Islam et al., 2015a). In biochar production, diverse feedstocks such as sawdust, crop residues, cattle manure, food wastes, moringa seeds, moringa leaves, and municipal wastes are mainly used (Islam et al., 2022; Kwak et al., 2019; Wang et al., 2020). Producing biochar from these wastes and applying them as remediation for wastewater is environmentally prudent and can be cost-effective. Table 1 summarizes the pyrolysis temperature and potential applications of biochar from different feedstocks.

Table 1. Different feedstocks, pyrolysis temperature, and potentials applications of biochar (Adopted from Roy et al., 2022a)

Feedstock for biochar preparation	Pyrolysis temperature (°C)	Potential or practical applications	Results	Reference
Coconut husk	378	The coconut husk-derived biochar was used to reduce nitrate leaching by slowing down nitrification in soil.	The biochar reduced both nitrifying archaea and bacteria abundance in soil by 71–83 % in the top 4 cm soil layer.	(Plaimart et al., 2021)
Yeast biomass	700-1000	The produced biochar was used for sulfonamide antibiotics degradation by peroxymonosulfate activation.	100% of sulfonamide removal was achieved in 20 min with a catalyst dosage of 0.4 g/L	(Peng et al., 2021)

Wheat Straw	300-700	The wheat straw biochar produced at 300 and 700 °C was used for the lead (II) adsorption from water	Sorption capacities of 55 and 109 mg/g were achieved for 300 and 700 °C, respectively	(Kwak et al., 2019)
Saw dust	700	Saw dust biochar produced at 700 °C was used for the lead (II) adsorption from water	A sorption capacity of 43 mg/g was achieved.	(Kwak et al., 2019)
Rice straw	600	Rice straw biochar produced at 600 °C was used for heavy metals removal from an aqueous solution	Sorption capacities were: Ni ²⁺ ~ 50 mg/g, Cd ²⁺ ~42 mg/g and Pb ²⁺ ~ 190 mg/g.	(Islam et al., 2021),
Willow wood	550	Willow wood-derived biochar was used for Cd ²⁺ removal	Cd ²⁺ sorption capacity was 35.7 mg/g.	(Zheng et al., 2020)
Biological sludge from paper mills	300-600	The produced biochar was characterized using different	Further analysis had to be done to verify the suitability of the biochar produced to be used in environmental applications, e.g., as soil amendment	(Tarelho et al., 2020)
Municipal and industrial sludge	500-700	The produced biochar had improved thermal stability, and efficient combustion	The biochar can be used for efficient combustion practices	(Chanaka Udayanga et al., 2019)

2.1.3 *Moringa oleifera*-derived adsorbents

M. oleifera is one of the most widely distributed species of the Moringaceae family throughout most parts of the world. In this context, *M. oleifera* seed is a widely available and inexpensive feedstock for producing biochar from pyrolysis (Bagheri et al., 2020). This feedstock has been used to produce biochar, extract and powder for different environmental applications such as soil amendment, metal sorption, and dye sorption in the aqueous phase (Ali, 2020; Kumari et al., 2006). Different preparation methods and performances of *M. oleifera*-derived adsorbents are summarized in Table 2. The adsorption capacity of biochar depends on its surface area, pore size, surface functional groups (e.g., carboxyl and hydroxyl groups), pH, and other physicochemical properties (Islam et al., 2022; Al-Mamun et al., 2021; Kwak et al., 2019). Different preparation methods and performances of *M. oleifera*-derived adsorbents.

Table 2. Preparation methods and performances of *M. oleifera* derived adsorbents (Adopted from Roy et al., 2022a)

Adsorbent type	Preparation method	Application	Removal performance	References
<i>M. oleifera</i> Lamarck seed powder	Crushed and sieved through copper sieves	Arsenic (As) from an aqueous system	85.6 %	(Kumari et al., 2006)
<i>M. oleifera</i> seed powder	Dry unshelled seeds were grounded and classified in two sizes (0.5 and 1.0 nm)	Ni (II) from aqueous solution	90 %	(Marques et al., 2012)
<i>M. oleifera</i> seed powder	Deshelled by hand and ground in the coffee mill until a consistent powder was obtained	Lead (Pb) from contaminated water	68.43 %	(Mataka et al., 2006)
<i>M. oleifera</i> seed powder	Washing, drying, grounded, and sieving to particle sizes 0.25-1.6 mm	Methylene blue and congo red from aqueous solution	90.27 % and 98.52%	(Raj et al., 2013)
<i>M. oleifera</i> seed powder	Dry unshelled seeds were grounded and applied	Congo red and dispersed red 60	170.7 and 196.8 mg /g	(Soliman et al., 2019)
<i>M. oleifera</i> seed powder	Seeds were crushed with mortar and pestle to obtain a fine powder	Tie and dye industrial effluent	65% decolorating	(Adesina et al., 2021)
<i>M. oleifera</i> seed extract	Powdered, made solution with 1 M NaCl, then stirred	Carmine Indigo Dye from aqueous solution	80 %	(Beltrán-Heredia et al., 2009)
Calcium-modified <i>M. oleifera</i> wood biochar	Pretreated with calcium and pyrolyzed in a furnace	Aqueous arsenate	37.22 mg/g	(Prasad et al., 2022)
<i>M. oleifera</i> seed biochar	Direct pyrolysis at 200 °C	Nitrobenzene from aqueous solutions	0.078 mg/g	(Tavengwa et al., 2016)
H ₃ PO ₄ modified <i>M. oleifera</i> seed	Produced by pyrolysis at 450 °C for 2 h at 10 °C/min	Diclofenac from an aqueous solution	100.88 mg/g	(Bagheri et al., 2020)

2.1.4 Modified biomass-based adsorbents

Raw biochar decontamination does not completely remove pollutants, but rather physically adsorbs them on the surface (Mohan et al., 2016; Islam et al., 2021b). As a result, researchers have been investigating the synthesis of a low-cost biomaterial adsorbent that can be used as an alternative to chemical adsorbents. However, the lack of efficacy of pristine biochar due to the low surface area, irregular pore distributions, and fewer surface functional groups, research on the surface modification of biochar have received a lot of attention in the last few decades (Wang et al., 2020). The sorption capacity of biochar can be increased by enhancing the surface area and functional groups by surface modification (Petrovic et al., 2022). The functional groups and surface area of biochar can be enhanced by different surface modification techniques. Different types of chemicals such as acids, bases, and salts were used to modify carbonized biochar surfaces. In recent years, along with chemical modification, natural polymers like polysaccharides have gained immense attention due to their availability, biodegradability, and enhanced activity. Chitosan-modified biochar is used for the adsorption of different organic and metal species (Liu et al., 2019). Modification of biochar by chitosan results in increased surface pore area and surface functional groups (Li et al., 2022). On the other side, modification of biochar by amphoteric oxide such as ZnO is already being used for the inherent synergistic and photocatalytic activity of ZnO to increase the activity of biochar (Al-Mamun et al., 2021b; Rashid Al-Mamun et al 2021).

2.2 Factors affecting of dye adsorption

Many factors influence dye adsorption, including solution pH, temperature, and initial dye concentration. As a result, the effects of these parameters must be considered. The optimization of such conditions will be extremely beneficial in the development of industrial-scale dye removal treatment processes. The factors influencing dye adsorption are discussed in the following section.

2.2.1 Effect of solution pH

The pH of a solution is one of the most important factors influencing adsorbent capacity in wastewater treatment. Changes in pH affect the ionization of the adsorbate and the surface properties of the adsorbent (Afroze et al., 2016). The Point of Zero Charges (pzc) signifies the surface's adsorption ability and the type of surface-active centers (Sun et al., 2019). The point of zero charges (pzc), indicates the pH at which the surface charge is zero and it is commonly used

to quantify a surface's electro-kinetic properties. The value of pH is used to describe pzc only for systems in which H^+/OH^- are the potential determining ions. There are many scientific studies on the point of zero charges (pzc) of various adsorbents to understand the adsorption mechanism. The Presence of the functional group; the OH^- group, defines that cationic dye adsorption is favored at $pH < pHPzc$, whereas, anionic dye adsorption is favored at $pH > pHPzc$.

2.2.2 Effect of initial dye concentration

The amount of dye removal depends on the initial dye concentration. The effect of initial dye concentration is related to the dye concentration and available sites on an adsorbent surface. In general, the percentage of dye removal decreases with the increase in initial dye concentration due to the saturation of adsorption sites on the adsorbent surface. On the other hand, an increase in initial dye concentration will result in an increase in adsorbent capacity because of the high driving force for mass transfer at a high initial dye concentration (Sabouni et al., 2019).

2.2.3 Effect of temperature

Temperature is an important physicochemical process parameter for changing the adsorption capacity of the adsorbent (Amar et al., 2021). Adsorption is an endothermic process where the amount of adsorption increases with increasing temperature due to the mobility of dye molecules and the number of active sites. On the other hand, when adsorption becomes an exothermic process reduces the adsorptive forces between the adsorbate and the active sites on the adsorbent surface, resulting in a decrease in adsorption capacity (Wang et al., 2019).

2.2.4 Effect of amount of adsorbent

The adsorbent's capacity is determined by adsorbent dosage at operating conditions. This is an important process parameter. The percentage of dye removal increases with increasing adsorbent dosage, as the number of sorption sites at the adsorbent's surface increases with increasing adsorbent dosage. The effect of adsorbent dosage provides an idea of a dye's ability to be adsorbed with the smallest amount of adsorbent and this indicates a dye's capability from an economic standpoint.

2.3 Selection of Synthetic Dye

In accordance with their raw ingredients, dyes are classified as natural and synthetic. Natural dyes are derived from vegetable and animal sources. Synthetic dyes are typically aromatic compounds including aromatic rings with delocalized electrons and various functional groups (Yaseen et al., 2019). For every dyeing industry, the use of synthetic dyes is most advantageous due to their availability, superior coloring, and low cost. The chromogen-chromophore structure (electron acceptor) is responsible for the color of dyes. The presence of auxochrome groups (electron donors) plays an important role in the dyeing ability. The electron acceptor is made up of an aromatic structure that is usually based on benzene rings. The electron donor is doubly conjugated with delocalized electrons, similar to an azo group (-N=N-). An auxochrome group is ionizable with control over dye-binding capacity. The -OH (hydroxyl) group is the most common type of auxochrome group (Alhelou et al., 2019). All of these structural characteristics make synthetic dye an excellent choice for textile dyeing. On the other hand, these same properties combine to become irrecoverable adverse costs for the environment. The textile industrial uprising has resulted in an alarming increase in the use of textile dyes. Currently, approximately 20% of total global dye production is released into the environment. The majority of the release occurs at some point during the dyeing process.

2.3.1 Azo Dyes

Azo dye is regarded as one of the most problematic dyes. The azo dye **has** numerous negative effects on the environment. First of all the aromatic ring structure **can** withstand biodegradation. Furthermore, the azo group becomes toxic amines easily as time has gone. These amines are carcinogenic and easily get access to the human food chain (Nanjani and Keharia, 2021). The chemicals cause allergies, dermatitis, malignant tumors, and cancer. Aside from these concerns, the LD₅₀ value for aromatic azo dyes ranges from 100 to 2000 mg/kg body weight. It is easily consumed by people whose water and food cycle have been contaminated by azo dye wastewater. Currently, azo dyes account for approximately 60-80 percent of the available dyes in the market. Based on the number of azo bonds present azo dyes are divided into three categories: mono-azo dye, di-azo dye, and tri-azo dye. Unfortunately, numerous types of azo dyes have been discovered to be harmful to the environment (Yu et al., 2012).

2.3.2 Methylene Blue

Methylene blue dye (MBD) is a heterocyclic aromatic chemical compound with the molecular formula of $C_{16}H_{18}N_3SCl$, the molecular weight is 319.85 g/mol, and the maximum wavelength, $\lambda_{max} = 663$ nm (Mahkooor et al., 2020). The structure of MB is shown in Fig.1.

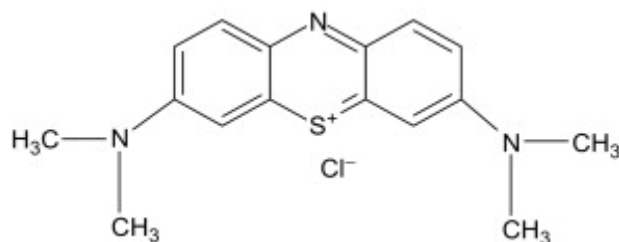


Fig. 1: Structure of Methylene blue

Methylene blue is a cationic dye of a thiazine nature and it is used to color paper, cotton, wool, and temporary hair colorants. MB was used in a variety of fields, including biology and chemistry. It appears as an odorless and dark green powder at room temperature (solid), and when dissolved in water, it produces a blue solution. This solution can be used as a redox indicator in analytical chemistry. Environmental scientists have recently expressed a strong interest in the removal of MB using modified biomass-based adsorbents.

2.4 Adsorbents Characterization and Analytical Techniques

Various analytical methods are used for adsorbent characterization, according to the literature. Many of these analytical techniques can now reach the molecular level. These analytical techniques help to understand precisely the nanoparticles. The universally reliable and splendid analytical techniques available for adsorbent analysis are stated below:

- Fourier Transform Infrared (FTIR) Spectroscopy
- X-Ray Diffraction (XRD)
- Nitrogen Physisorption Measurement (BET analysis)
- Scanning Electron Microscope (SEM)
- UV-VIS Spectrophotometer

2.4.1 Fourier Transform Infrared (FTIR) Spectroscopy

Fourier Transform Infrared Spectroscopy helps to obtain an infrared spectrum of absorption of a solid, liquid or gas. FTIR is an excellent technique for recording between 4000 cm^{-1} and 400 cm^{-1} spectra for qualitative analysis. It simultaneously collects high-resolution spectral data over a wide spectral range. The raw data is processed with the help of the Fourier Transform algorithm. Functional groups are investigated with FTIR for different IR regions in response to the corresponding molecular vibrations. The different intense spectrum peaks indicate the nature of the materials present (Torres-Cruz et al., 2020).

2.4.2 X-Ray Diffraction (XRD)

X-ray diffraction (XRD) helps to investigate the crystalline structure and composition of a substance which is based on the interaction of a monochromatic x-ray beam with the crystal lattice. The episodic arrangement of atoms in three dimensions is characterized by crystal lattice structures of substance where the atoms can diffract or scatter any type of light beam. Under sophisticated controlled conditions, the diffracted beams follow the interference properties of a wave. For a composite, the maximum interference corresponds to the same symmetry of distributed atoms. Bragg's law can explain this decisive factor for constructive interference. The law is represented by the equation:

$$2d \sin\theta = n\lambda \quad (2.1)$$

where 'd' is the lattice plane space, 'θ' is the angle of diffraction, 'n' is the order of diffraction, and 'λ' is the x-ray wavelength.

2.4.3 Nitrogen Physisorption Measurement (BET analysis)

The Brunauer-Emmet-Teller technique is used to determine the porosity and surface area of microporous and mesoporous materials. Porosity and surface area are essential parameters for adsorption studies as they indicate the structural properties of the adsorbents and may even reveal the sites for possible adsorption. BET method is applied to characterize the effect of adsorption on pore size distribution, pore volume, and the surface area of adsorbents (Virtanen et al., 2020)

2.4.4 UV-VIS Spectrophotometer

The spectrophotometer represents the optical concepts. It measures the interaction of light beams of different wavelengths with liquids and solids. The wavelength region represents various types of optical transitions and interactions with solids and liquids. Reflectance against wavelength curves is easily observed in solid-like semiconductors. The absorbance is calculated using the reflectance values. The absorbance curve is used to track the shift in the absorbance edge. The chemical compounds present in the liquid trigger light absorbance. This absorbance property defines the specific compounds in liquid mixtures. At the same time, Beer's law can be used to calculate the concentration of that specific compound. Beer's law is represented by the equation: $A = bC$; the absorbance quantity (A) of a solution is proportional to the concentration of the absorbing species (C) where the path length (b) is constant.

2.4.5 Scanning Electron Microscope (SEM)

A scanning electron microscope (SEM) is used to capture high-resolution surface images of samples. An ordinary SEM is thought to be capable of producing images at the nanoscale level. Electrons are of high-energy focused over the sample, scattering from the solid surface, in SEM and SEM images are created by scanning. The visual understanding and identification of structural morphology is the primary advantage of SEM images. Detailed information about the roughness, shapes, and distribution of the sample's constituents can be found in the SEM image.

CHAPTER 3

METHODOLOGY

3.1 Materials

The chemicals used for the experiment include Zinc nitrate hexahydrate $\{Zn(NO_3)_2 \cdot 6H_2O\}$ [Sigma-Aldrich], chitosan [Sigma-Aldrich], acetic acid (CH_3COOH) [Merck, 99.5%], methylene blue [Sigma-Aldrich, dye content 85%], caustic soda ($NaOH$) [Sigma-Aldrich] and nitric acid (HNO_3) [Merck, 69%]

3.2 Experimental methods

The experimental methods and procedures are determined by taking research objectives into consideration. The main aim was to synthesize CZB as a ternary composite. The major parts of this particular research were divided into segments shown below:

- Preparation of Biochar from *M. oleifera* seed
- Preparation of Biochar/Chitosan, Biochar/ ZnO , and Chitosan/ ZnO as binary composites
- Preparation of Chitosan/Biochar/ ZnO as ternary composite
- Characterization of the binary and ternary adsorbent materials
- Adsorption of methylene blue

The features of all these methods are discussed in detail in the following sections.

3.2.1 Biochar(B) preparation

Dry seeds of *M. oleifera* were initially washed with ethanol to wash out the organic impurities and then dried in an air oven to bring out the moisture content $\leq 10\%$. The dried seeds were then crushed with a grinder and then 10 g of ground mass was fed into an N_2 furnace (Nobetherm P 300, Germany). Before heating the furnace, a 1.0 Lh^{-1} flow of N_2 gas was maintained to purge the furnace. There was a continuous N_2 flow (0.6 Lh^{-1}) at about 350°C with a heating rate of $5.8^\circ\text{C min}^{-1}$ at 2 bar pressure for 3h. After that, the biochar sample was taken out and then purified with 15% nitric acid (HNO_3) solution under stirring at 40°C for 4 hrs., which will help to oxidize some functional groups of the biochar surface to improve its functionality. Then the sample was washed with deionized water and finally neutralized material was dried at 105°C for 12 h.

3.2.2 Biochar/chitosan (BC) preparation

1 g of chitosan was dissolved in 180 mL acetic acid (2%) and 3 g of the biochar was then be added to the solution. The mixture was stirred vigorously for 30 min. Then the biochar-chitosan homogenous suspension was added drop wise into a 900 mL NaOH (1.2%) solution and kept in the solution for 12 h. The chitosan-modified biochar was then washed with deionized (DI) water to remove the excess NaOH and oven-dried for 24 h at 105°C.

3.2.3 Biochar/ZnO (BZ) preparation

The biochar modified by ZnO particles (BZ) was prepared by impregnation of the biochar powder into Zn (NO₃)₂ aqueous solutions. Initially, biochar was pretreated using zinc nitrate solution (the mass ratio was 1 : 1). After the addition of Zn (NO₃)₂, the adsorbent was dried at 105°C for 12 h. Then the Zn(NO₃)₂-pretreated biochar was mixed with 0.1 M NaOH and then pyrolyzed at 380°C for 1 h under an N₂ atmosphere to obtain BZ. Subsequently, the sample was naturally cooled to ambient temperature to obtain the final adsorbent.

3.2.4 Chitosan/ZnO (CZ) preparation

2.0 g of ZnO powder was dissolved in 100 mL of 1% (v/v) acetic acid where ZnO reacted with acetic acid and changed to zinc cations (Abdelhady, 2012). Then 1.0 g of chitosan was added to the mixture solution. The mixture was sonicated for 30 min in a frequency sonicated bath. After magnetic stirring, 0.10 M NaOH was added drop by drop until the solution obtained pH=7. The solution was heated in a water bath at 75-80°C for about 3 h. Next, the solution was filtered and washed with distilled water several times before being dried in an oven at 50°C for 1 hour.

3.2.5 Chitosan/ZnO/biochar preparation (CZ-B)

For the preparation of the CZ-B composite, 1 g of CZ composite was dispersed in water. 1 g of biochar was then added to the suspension. The suspension was then exposed to ultrasonic vibration for 1 hr. The composite was then washed with acetic acid solution and water for purifying unreacted chitosan. The sample was then pyrolyzed at 350°C for 1 h under N₂ atmosphere to obtain BZ. The sample was naturally cooled to ambient temperature to obtain the final adsorbent.

3.3 Characterization of adsorbents

Different characterization techniques were used to confirm the successful preparation of *M. oleifera*-derived biochar and other composites. In the experiments, chitosan and ZnO were used as purchased, so these samples were not characterized. Fine particles of Biochar, BC, BZ, CZ, and CZ-B samples were used for Fourier transform infrared spectroscopic (FTIR) analysis. A small amount of prepared material was mixed with KBr powder for making pellets. FTIR spectra were recorded in the range of 4000–400 cm^{-1} in transmission mode using an FTIR-8400 instrument (Shimadzu, Japan). Surface textures of the prepared materials were recorded using a field emission scanning electron microscope (FESEM), JSM-7600F (JEOL, Japan) at a 10.0 kV operating voltage with 1 nA probe current and 0–20 KeV energy range. A drop of the dilute aqueous suspension of the samples was taken in a glass plate and vacuum dried, and the surface was coated with a thin layer of gold. X-ray diffraction (XRD) patterns of the samples were recorded using an X-ray diffractometer (RIGAKU Ultima IV, X-ray Diffractometer, Japan), with a Cu X-ray source (1D scan, 40 kV and 40 mA X-ray generator)) in the 10 to 80° 2θ range. The scan speed of 10.00° min^{-1} and step width of 0.02° was used for the testing. The Brunauer-Emmett-Teller (BET) surface areas were measured with N_2 adsorption at 77 K using a surface area analyzer (PulseChemiSorb 2705, micromeritics Instruments, BUET, Bangladesh). Initially, the samples were weighed and degasified at 180°C for 1 h. Then the adsorption and desorption cycles were carried out with 15%, 30%, 50 %, and 90% N_2 concentrations respectively to find out the surface area.

3.4 Experimental Design

The adsorption behaviors of biochar, chitosan, ZnO, BC, BZ, CZ, and CZ-B were studied systematically with different solution pH, adsorption time, and initial dye concentration. By changing the initial pH value from 3.0 to 11.0, the effect of pH on adsorption was investigated. Adsorption kinetic studies were carried out at room temperature with an initial dye concentration of 60 ppm, and independent samples were measured at time intervals ranging from 15 to 180 minutes. For 90 min, adsorption isotherm experiments were carried out with various initial dye concentrations ($C_0 = 10\text{--}70 \text{ mgL}^{-1}$). The precipitate was separated, and the supernatant solution's residual concentration was determined using a UV–Vis spectrophotometer (SHIMADZU UV-

1601). The dye's removal (percentage) and equilibrium adsorption capacity (q , mgg^{-1}) were calculated using Eqns. (1) and (2), respectively (Niasar et al., 2019).

$$\text{Removal, \% } R = \frac{(C_i - C_e) \times 100}{C_i} \quad (1)$$

$$\text{Adsorption Capacity, } q \left(\frac{\text{mg}}{\text{g}} \right) = \frac{(C_i - C_e) \times V}{m} \quad (2)$$

Where C_i and C_e are the initial and equilibrium concentrations (mL^{-1}) of MB dye in the aqueous solution, respectively. q is the adsorption capacity (mgg^{-1}) of the adsorbents, V is the volume of the dye solution (L), and m is the mass of biochar (g) used for adsorption.

3.5 Statistical Design

Design-Expert Software (version 6.0.11) was used to analyze statistical experimental data. Response surface methodology investigated the effect of independent variables, including time (X_1), dye concentration (X_2), and pH (X_3) on the response variable, removal (%) by CZ-B. RSM design along with coded and uncoded levels is summarized in Table 3

Table 3. Independent variables and their corresponding levels for removal (%) (Adopted fom Roy et al., 2022a)

Independent variable	Symbol	Coded levels				
		$-\alpha$	-1	0	+1	$+\alpha$
Time (minutes)	X_1	7.5	10	65	120	157.5
Concentration (mg/L)	X_2	9.5	10	35	60	77.0
pH	X_3	0.7	2	6	10	12.7

Central composite design and quadratic model were used to design this experiment. Twenty treatments, including six axial points, eight fractional factorial points, and six central points were randomly performed according to CCD. To understand the effect of operating variables on response variables, response plots were generated using Design-Expert Software (version 6.0.11).

3.6 Isotherms and kinetics modeling

3.6.1 Isotherms

3.6.1.1 Langmuir isotherm model

This model is commonly used for homogeneous adsorption processes. It implies that the adsorbent's surface has a limited number of active sites that are equally accessible to each dye molecule. Each active site has the same affinity for the dye molecules, has the same thermal energy, and contains the same number of molecules. This allows for uniform monolayer adsorption. It also assumes that when a dye molecule occupies an active site on the surface, no additional adsorption occurs at that specific site. There is no interaction between the adsorbate molecules or neighboring active sites, such as steric hindrance. There is a dynamic equilibrium point in the model where the rates of adsorption and desorption are the same. The physical significance of this phenomenon is that all active sites on the surface have been occupied, resulting in saturation (Auta & Hameed, 2012).

The non-linear form of the Langmuir model is,

$$Q_e = \frac{Q_m K_L C_e}{1 + K_L C_e} \quad (3)$$

The linear form is,

$$\frac{C_e}{Q_e} = \frac{1}{Q_m K_L} + \frac{C_e}{Q_m} \quad (4)$$

Here, K_L = Langmuir isotherm constant (Lmg^{-1})

Q_m = the maximum adsorption capacity (mgg^{-1}).

C_e = the dye concentration in equilibrium (mgL^{-1}),

Q_e = adsorption capacity of AC (mgg^{-1}),

A plot of $\frac{C_e}{Q_e}$ vs. C_e is drawn. This model developed a separation factor R_L that can be described as follows,

$$R_L = \frac{1}{C_0 K_L + 1} \quad (5)$$

This separation factor can be calculated if the experimental data fit well. Here, C_0 denotes the initial dye concentration (mgL^{-1}). The value of R_L indicates whether the adsorption is favorable or unfavorable. If the value of $R_L = 0$, the process is irreversible, $R_L = 1$, the process is linear and the value of R_L is between zero and one, the process is considered to be favorable. A value greater than one indicates that the condition is unfavorable (Sewu et al., 2019).

3.6.1.2 Freundlich isotherm model

This empirical model was developed on the basis of heterogeneous adsorption. It, unlike the Langmuir isotherm, is not limited to ideal adsorption and can also be used to describe non-ideal adsorption. It is based on multilayer adsorption with a varying affinity for dye molecules and non-uniform enthalpy distribution across the adsorbent surface. The dye uptake by the AC increases with increasing dye concentration, implying an infinite supply of active sites. Each active site has a unique binding energy, and the ones with the highest binding energy are occupied first. As a result, the total amount of dye molecules extracted is calculated as the sum of all adsorption on the AC surface. However, as adsorption progresses, the adsorption energy decreases dramatically. The non-linearized form of Freundlich isotherm model is as follows,

$$Q_e = K_F C_e^{\frac{1}{n}} \quad (6)$$

The linearized form is,

$$\ln Q_e = \ln K_F + \frac{1}{n} \ln C_e \quad (7)$$

Here, Q_e = adsorption capacity of AC (mgg^{-1}),

C_e = the dye concentration in equilibrium (mgL^{-1})

K_F = Freundlich isotherm constant (mgg^{-1}) (Liu et al., 2019)

A plot of $\ln Q_e$ vs. $\ln C_e$ can provide the value of $1/n$ and K_F . When the temperature increases, the values of K_F and n can vary, indicating that the amount of dye adsorbed grows more gradually and that pressure increases are required to bring the adsorbent surface into equilibrium (Yagub et al., 2012)

The slope is $1/n$ is called the Freundlich intensity parameter and it lies between 0 and 1. The value of n denotes the degree of heterogeneity on the surface of the adsorbent; the greater the value of n , the greater the degree of heterogeneity. The significance of the slope is shown in Table 4, (Foo & Hameed, 2010, Sewu et al., 2019).

Table 4. Significance of slope $1/n$

$1/n = 0$	Irreversible
$1/n < 1$	Favorable (chemisorption process)
$1/n = 1$	Linear
$1/n > 1$	Unfavorable (cooperative adsorption)

While this model is advantageous for systems with heterogeneous and non-ideal features, it violates a fundamental thermodynamic property known as Henry's law at low concentration, which is a disadvantage.

3.6.1.3 Temkin isotherm model

This is another well-known isotherm model that, unlike the previous two, includes the indirect interaction of the adsorbent and dye molecules. It explicitly accounts for adsorbent–adsorbate interactions and adsorption energy while the binding energies of active sites can vary, they do so uniformly. This model assumes that the heat of adsorption of all molecules in the layer decreases linearly with the surface area covered due to adsorbent–adsorbate interactions. The adsorption is distinguished by a uniform distribution of binding energies up to maximum binding energy. The Temkin isotherm is derived on the assumption that the decrease in heat of sorption is linear rather than logarithmic, as implied by the Freundlich equation. It is particularly good at predicting gas phase equilibrium and complex adsorption systems.

$$Q_e = \beta \ln A_t + \beta \ln C_e \quad (8)$$

Where $\beta = \frac{RT}{b_T}$ Q_e = adsorption capacity of AC (mg/g), b_T = the Temkin isotherm constant, C_e = the dye concentration in equilibrium (mgL^{-1}), A_t = the Temkin isotherm equilibrium binding constant (L/g), T = the absolute temperature (K), β = the constant related to the heat of adsorption (J/mol) and R = universal gas constant ($8.314 \text{Jmol}^{-1}\text{K}^{-1}$) (A.O, 2012). The plot of Q_e vs. $\ln C_e$ provides the values of β and A_t (Inam et al., 2017).

3.6.2 Adsorption Kinetics

3.6.2.1 Pseudo-first-order adsorption kinetics

The differential form of the pseudo-first-order process is as follows,

$$\frac{dq_t}{dt} = k_1 (q_e - q_t) \quad (9)$$

Here, q_e = amount of dye removed in equilibrium (mgg^{-1})

q_t = the amount of dye removed over time t (mgg^{-1}),

k_1 = equilibrium rate constant for the pseudo-first-order process (min^{-1}).

Integration of these differential forms leads to a linearized equation which is as follows (Khan, 2019),

$$\log \left(\frac{q_e}{q_e - q_t} \right) = \frac{k_1 t}{2.303} \quad (10)$$

This is known as Lagergren's pseudo-first-order kinetic model. The majority of adsorption processes have diffusion as the dominating mode of mass transfer. The first-order equation helps to portray experimental kinetic data. One of the limitations of this model is that sometimes only fits well for the short initial period of contact. (Shuhan et al., 2021, Foo & Hameed, 2010).

3.6.2.2 Pseudo-second-order adsorption kinetics

The differential form of the pseudo-second-order process is as follows

$$\frac{dq_t}{dt} = k_2 (q_e - q_t)^2 \quad (11)$$

Here, k_2 is the equilibrium rate constant for the pseudo-second-order process ($\text{gmg}^{-1} \text{min}$) and q_t and q_e has their usual meanings. Integrating the differential form leads to the linearized form which is as follows (Yao et al., 2020)

$$\frac{t}{q_t} = \frac{1}{k_2 q_e^2} + \frac{t}{q_e} \quad (12)$$

The Chemisorption mechanism is used in this case and is the rate-limiting stage in the entire process. In contrast to the pseudo-first-order model, the pseudo-second-order model is capable of anticipating the system's behavior throughout the whole contact time. The model has the advantage of being able to estimate the adsorption capacity and initial adsorption rate without the need to identify any unknown parameters first. (Shuchi et al., 2021, Foo & Hameed, 2010).

CHAPTER 4

RESULTS AND DISCUSSION

4.1 Characterizations of synthesized materials

Fig 2 shows the FTIR spectra of biochar, BC, BZ, CZ, and CZB respectively. In the FTIR spectrum of biochar adsorption peaks around 2923 and 2860 cm^{-1} can be attributed to C-H symmetric and asymmetric stretching, respectively. The peak around 1600 cm^{-1} corresponded to the C=O stretching and aromatic C=C vibrations. The wide peak at 3430 cm^{-1} corresponds to the O-H stretching vibration of H₂O. In the FTIR spectrum of BC, the band at 1084 cm^{-1} corresponds to the free amino group at C₂ of glucosamine (Janu et al., 2021). A peak at 1375 cm^{-1} was observed corresponding to the C-O stretch in the primary alcoholic group of chitosan. The OH stretching frequency at 3425 cm^{-1} and also the CO (amide) and NH primary amine bends were observed at 1615 cm^{-1} (Varma & Vasudevan, 2020). In the FTIR spectrum of BZ composite, the major absorption peaks were observed in the region of lower wave number due to the ZnO incorporation. A characteristic band observed at 900 and 539 cm^{-1} corresponds to the Zn-O stretching bond. The band observed at 1028 cm^{-1} may represent alcohols and phenolic groups (Jan et al., 2020). In the CZ composite, the presence of residual N-acetyl groups was confirmed by the bands at around 1383 cm^{-1} (C-N stretching of amide III (Beil et al., 2012, Fernandes Queiroz et al., 2014)); the peaks at 2930 and 2860 cm^{-1} are attributed to the C-H stretching vibration; and the peaks at around 1167 cm^{-1} may refer to the C-O stretching vibration; peaks around 450 cm^{-1} referring to the Zn-O stretching (Pandiyarajan & Karthikeyan, 2013, Kumar et al., 2011) Compared to biochar, the CZB exhibits the characteristic peaks at 1383 cm^{-1} , which indicates the C-N stretching and peaks around 450 cm^{-1} validate the presence of Zn-O stretching. The peak at 3710 cm^{-1} may attribute to the hydroxyl stretching vibration of free phenol groups and water.

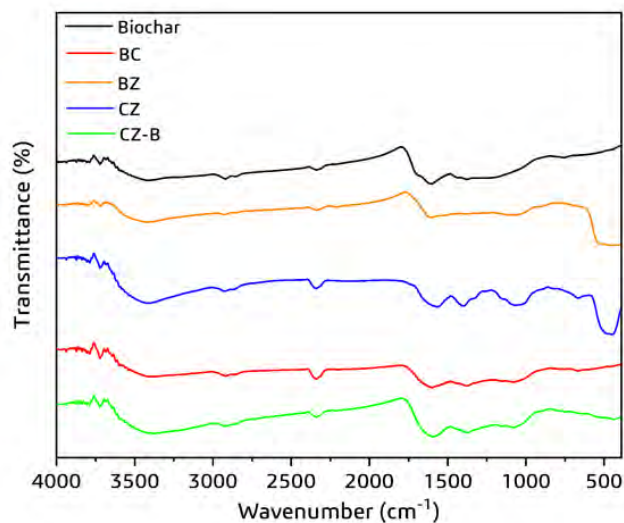


Fig. 2. Comparison of the FTIR spectra of Biochar, BC, BZ, CZ and CZ-B (Adopted from Roy et al., 2022b)

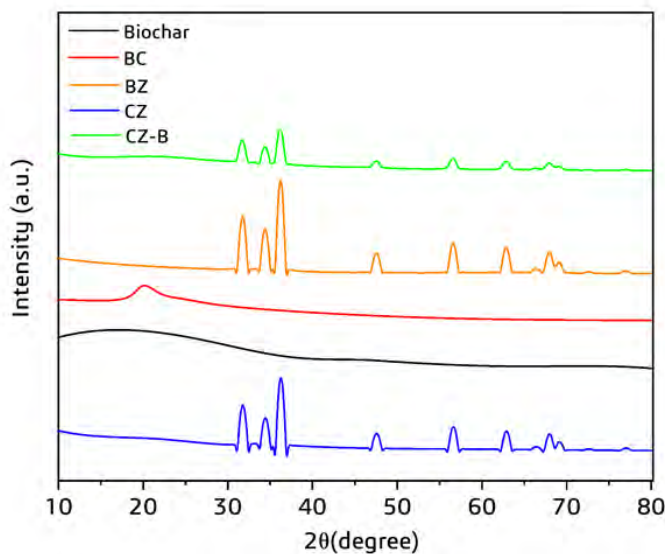


Fig. 3. XRD images of biochar, BC, BZ, CZ and CZ-B (Adopted from Roy et al., 2022b)

The XRD pattern of synthesized adsorbents is shown in Fig 3. The biochar particles were observed to be fully amorphous having no sharp peak due to the decomposition of cellulose (Nartey & Zhao, 2014, Clemente et al., 2018). The XRD pattern of BZ composite has ten diffraction peaks with two intense peaks at $2\theta \sim 31.7^\circ$ and $\sim 36.25^\circ$. Those peaks correspond to the diffraction of the (1 0 0) and (1 0 1) planes respectively. The presence of the peaks confirms that the material exhibits a

typical nonlinear 3D carbon with an extremely disordered structure. The average crystallite size of prepared CZ nanoparticles was calculated at about 40.0375 nm by using this equation-

$$d = \frac{K*\lambda}{FWHM*\cos(\theta)} \quad (13)$$

Sharp peaks at 31.765°, 34.425°, 47.537°, 56.591°, 62.850° and 67.943° were assigned to the (1 0 0), (0 0 2), (1 0 2), (1 1 0), (1 0 3), and (1 1 2) planes of hexagonal zinc oxide can be indexed to the ZnO with high crystallinity (Abdelhady, 2012). The CZ-B composite is highly crystalline, and the average crystallite size of CZ-B was found 22.218 nm. It is evident that the presence of CZ as a stabilizer in biochar, which reduced the crystallite size of CZ-B. The diffraction peaks of CZ-B are in good agreement with those of the CZ structure and it indicates a successful formation of the CZ-B complex.

The surface morphologies of biochar, BC, BZ, CZ and CZ-B were investigated by FESEM. The FESEM images (Fig 4) and energy-dispersive X-ray spectroscopy (EDS) (Fig 5) of Biochar, BC, BZ, CZ and CZ-B are presented respectively. The surface morphology of biochar revealed the presence of macropores and irregular trough-like cracks, due to the decomposition and volatilization of raw materials (Fig. 4(a)). It is believed that the cracks were a result of high temperature, where the macropores were produced by destroying the walls of adjacent micropores, which decreased the surface area of biochar. The irregularly shaped carbon particles can be seen in Fig 4(b) of BC particles. Smooth surfaces with some rough cracks, irregular blocks, some crystalline clusters, disordered membrane fissures, no significant pores and no specific existence of chitosan particles are the main features of BC surface. The higher O% in the BC surface than biochar surface can be observed from the EDS results (Fig. 5(b) and Table 5) may indicate the increased functionalities of BC. The possible presence of -COOH and -OH groups can be predicted from this (Eddy et al., 2020).

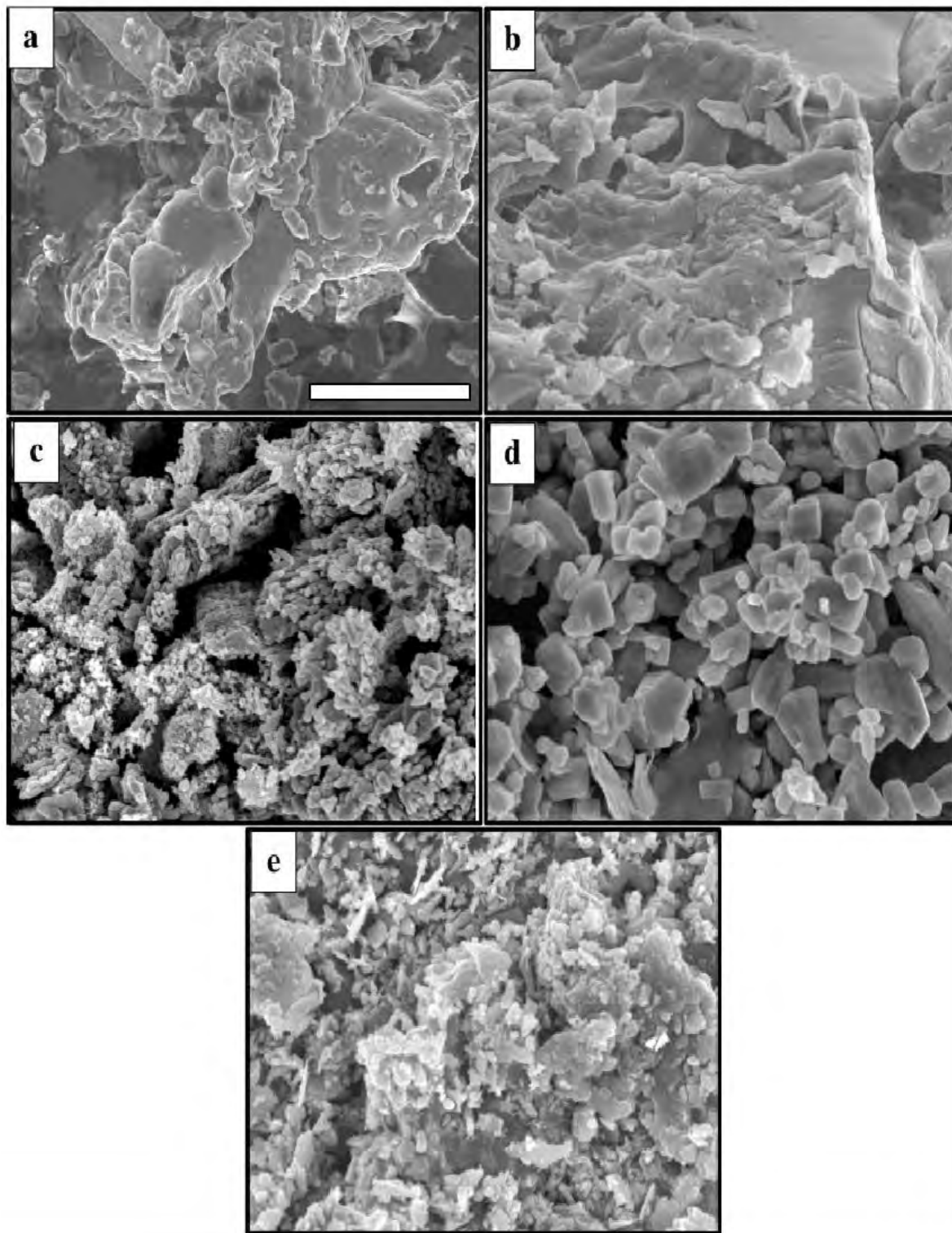
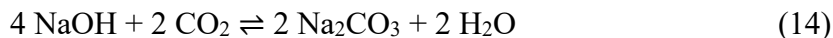


Fig. 4. Scanning electron microscope (SEM) micrograph ($\times 20000$ magnification) and bar of 10 micrometer (Adopted from Roy et al., 2022b)

The coral-shaped random 3D carbon particles can be observed in Fig 4(c) of the BZ composite. The incorporation of ZnO created tunnel-like cracks in the surface. The spherical-shaped clusters of ZnO can be visible in the SEM image. The ZnO nanoparticles may provide the nucleation center for pyrolysis which results in the formation of cracks around ZnO. C, O, Zn and a very trace amount of N were found in the BZ sample (Geetha et al., 2016). According to the EDS (Fig 5(c) and Table 5) report the weight percentage and atomicity of C, O, and Zn were found to be 14.94, 46.21 and 37.21. Another possible reason for pore formation in the BZ composite may be at this higher temperature and pressure it may react with the NaOH, which ultimately results in the rough surface, the macropores, and micro-sized channels by CO₂ diffusion through internal structures (Eqns. 14 and 15).



The FESEM images and EDS results of the CZ nanocomposite can be seen in Fig 4(d) and 5(d) respectively, it can be seen the particles appeared to be ordered in shape with quite distinct and uniform orientation. (Fig. 4(d)). From the EDS results of CZ, the presence of 26.11% Zn is observed. The FESEM image of the ternary composite CZB can be seen in Fig 4(e). After the addition of CZ composite into biochar, it was observed that the porous and irregular shape of biochar converted into agglomerated form. It is due to the addition of CZ into biochar produced larger chunks, where chunks of porous rock formed. The ZnO possibly provided the nucleation center, as a result, agglomeration occurs between ZnO and chitosan (Zhou et al., 2013). In the EDS results in Fig 5(e) and Table 5, the Zn content in CZB was found to be 18.28 %, which was smaller than the Zn content of BZ and CZ composites.

Table 5. Elemental composition of prepared samples from Energy -dispersive X-ray spectroscopy (EDS) (Adopted from Roy et al., 2022b)

Adsorbents	Elements			
	C (%)	N (%)	O (%)	Zn (%)
Biochar	70.35	17.35	12.30	-
BC	70.08	12.29	17.62	-
BZ	14.94	1.63	46.21	37.21
CZ	57.22	2.78	13.89	26.11
CZB	48.12	5.81	27.79	18.28

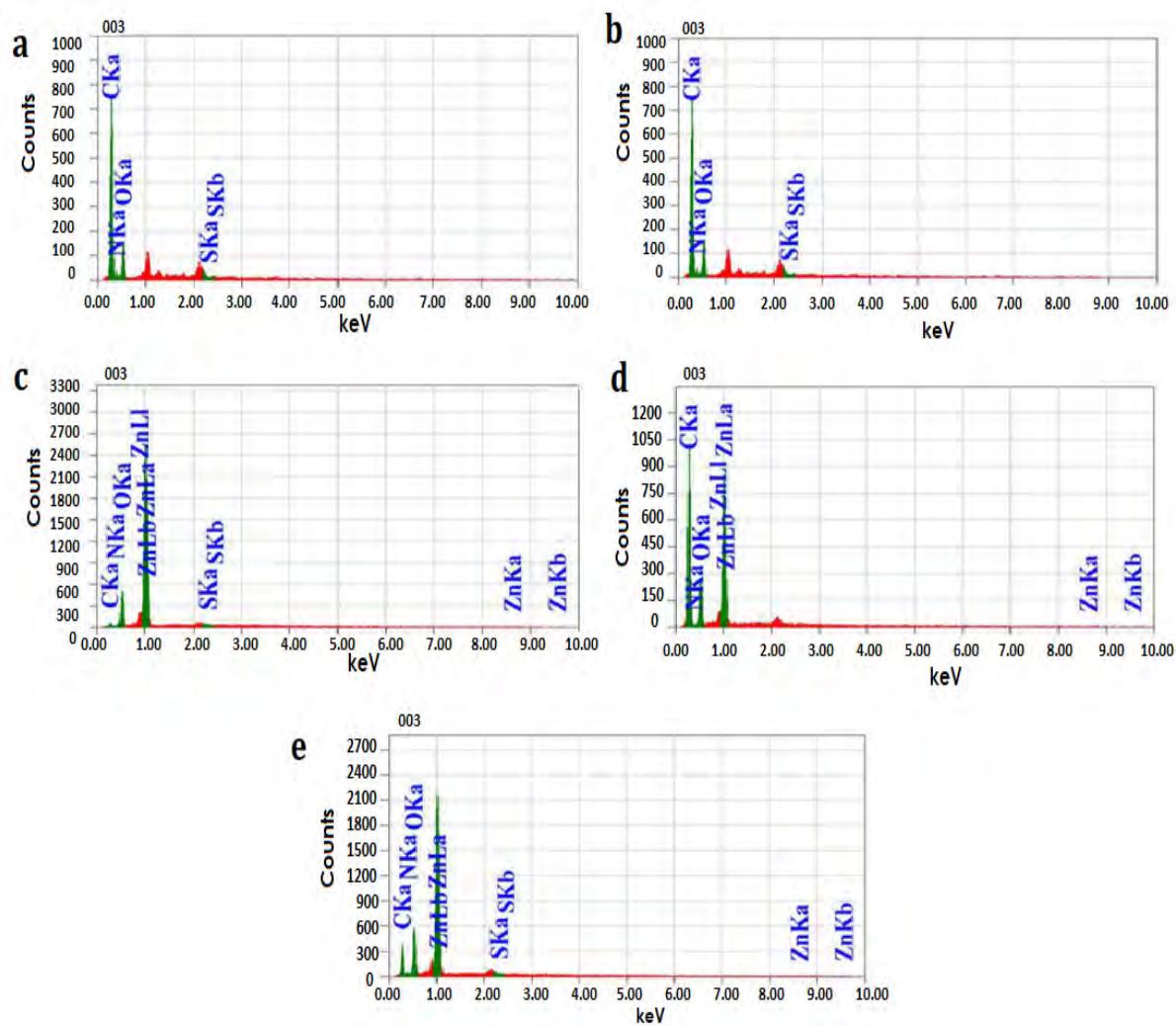


Fig. 5. Energy -dispersive X-ray spectroscopy (EDS) spectra of biochar (a), BC (b), BZ (c), CZ (d) and CZ-B (e)

Table 6. BET surface area of biochar, BC, BZ, CZ and CZB. BC stands for Biochar-chitosan, BZ stands for Biochar-ZnO, CZ stands for chitosan-ZnO and CZB stands for chitosan-ZnO/biochar. (Adopted from Roy et al., 2022b)

Adsorbents	Surface area (m ² g ⁻¹)
Biochar	0.96 ± 0.00
BC	0.90 ± 0.01
BZ	14.48±1.03
CZ	1.99 ±0.00
CZB	5.31 ± 0.00

Table 7. The average particle size of biochar, BC, BZ, CZ and CZB from the SEM image

Adsorbents	Average particle size (nm)
Biochar	32.03
BC	35.74
BZ	19.43
CZ	25.14
CZB	22.02

Table 6 and Table 7 summarize the measured BET surface area of biochar, BC, BZ, CZ, and CZB. The highest surface area was found for BZ, which is $14.48 \pm 1.03 \text{ m}^2 \text{ g}^{-1}$ with the lowest average particle size of 19.43nm and the lowest surface area was found for BC, which is $0.90 \pm 0.01 \text{ m}^2 \text{ g}^{-1}$ with the highest average particle size of 35.74nm. The FESEM images of the prepared adsorbents support the BET surface area results. The chitosan combined BC composite exhibited a decrease in the surface area, which may be caused due to the pore blockage of biochar. The ZnO incorporation significantly increased the surface area. This could happen due to the nucleation of

ZnO which introduced several micropores in the BZ structure. The ternary composite CZB exhibited a surface area of $5.31 \pm 0.00 \text{m}^2\text{g}^{-1}$, which was smaller than the surface area of BZ but higher than that of the CZ composite. Moreover, the average particle size of CZB found about 22.02nm, which was larger than that of BZ but smaller than that of CZ. From EDS results it can be seen that the O and Zn % have a direct contribution to the surface area. The average particle size of adsorbents was derived from SEM images by using ImageJ software.

4.2 Impact of pH

The initial pH of the dye solution modifies the surface charges and functionalities. The adsorption capacities of the prepared biochar at five different pHs e.g., 3,5,7,9, and 11 were derived and shown in Figure 6. It has been reported that the pH of the aqueous solution affects the sorption of contaminants onto biochar and its composites. This is related to the oxygen-containing functional groups, which are pH-dependent. Consequently, the surface charge and ionization at the surface of the adsorbents are pH-dependent leading to differentiating adsorption capacity of cationic MB dye contents. From fig.6 a deprotonation of the functional groups occurred when the pH of the aqueous solution increased. This led to the increase in the sorption capacity of the adsorbents towards cationic dye. On the other hand, when the pH decreased, it led to an increase in the electrostatic repulsion forces between the protons and cations in the aqueous solution. Consequently, it led to a decrease in the capacity of the adsorbent materials for dye removal%. When the pH solution became more alkaline the adsorption of dyes also increased due to the high interaction between the negatively charged sites on the adsorbents' surface with the positively charged dyes. In contrast, at pH=3, its efficiency to adsorb organic dye decreased because of the existence of extra H^+ that competes with the positive charges of the dye.

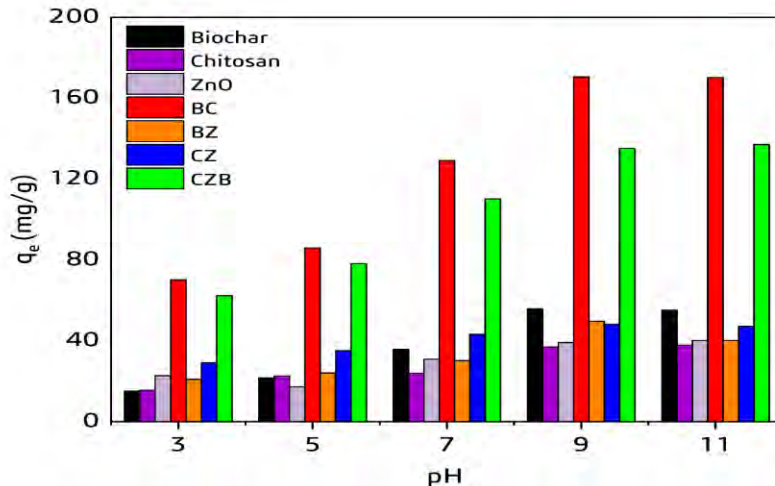


Fig. 6. Effect of pH on adsorption of MB by Biochar (black), Chitosan (purple), ZnO (light purple), BC (red), BZ (orange), CZ (blue) and CZB (green)

4.3 Effect of Contact Time and Adsorption kinetics

The effect of contact time at seven different time intervals e.g., 15, 30, 45, 60, 75, 90, 120 and 180 minutes on the q_t values at 25°C is shown in Fig. 7. The dye molecules rapidly adsorbed in the first 1–20 min, the adsorption rate then decreased gradually and reached equilibrium in about 90 min. In the beginning, the uptake rate for dyes was very high as many available adsorption sites for dye molecules. As the sites were gradually filled up, adsorption became slow due to dye aggregation at the surface. This aggregation caused difficulties for dye molecules to diffuse deeper into the adsorbent pores. The linear kinetics plots are presented in Figures 8 (a), and (b), and the parameters are summarized in Table 8. The R^2 value of the pseudo 2nd order model is close to unity (0.99) which justifies its viability with the actual adsorption phenomenon. The pseudo-second-order plot in Fig.8(b) represents a more orderly linear orientation of the data than the pseudo 1st order plot in Fig. 8(a). The maximum adsorption capacity, $q_{e, cal}$ for the pseudo 1st order model is 208.8 mgg^{-1} , which has a high deviation from the actual adsorption value. On the other hand, for the pseudo 2nd order model the $q_{e, cal}$ shows more closeness to the value derived from the experiment. The alignment of the kinetics parameters with the pseudo-second-order model suggests that the adsorption process is controlled by chemical interactions.

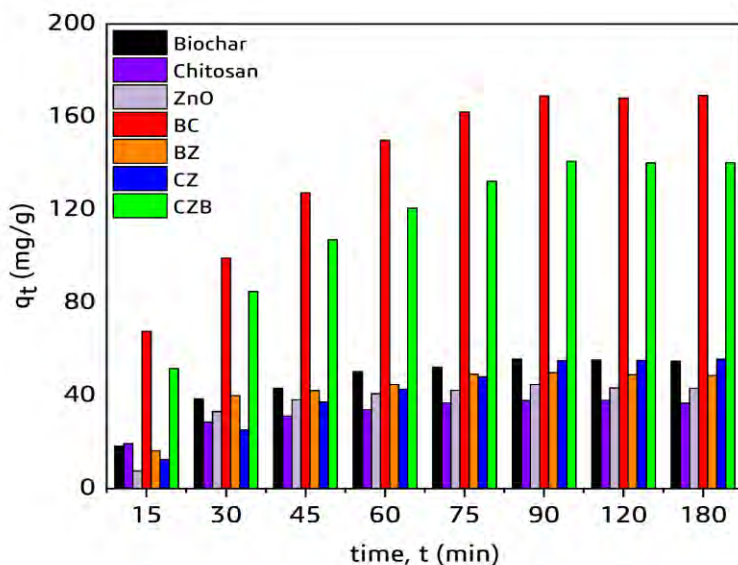


Fig. 7. Effect of time on adsorption of MB by Biochar (black), Chitosan (purple), ZnO (light purple), BC (red), BZ (orange), CZ (blue) and CZB (green)

Table 8. Kinetics modeling parameters obtained for pseudo-1st order, pseudo-2nd order model. BC stands for Biochar-chitosan, BZ stands for Biochar-ZnO, CZ stands for chitosan-ZnO and CZB stands for chitosan-ZnO/biochar. (Adopted from Roy et al., 2022b)

Adsorbents	Pseudo-1 st order				Pseudo-2 nd order		
	q _e exp (mgg ⁻¹)	R ²	q _e calc (mgg ⁻¹)	k ₁ (min ⁻¹)	R ²	q _e calc (mgg ⁻¹)	k ₂ (g.mg ⁻¹ min ⁻¹)
Biochar	55.70	0.82	49.40	0.058	0.95	60.60	4.95×10 ⁻⁴
Chitosan	38.15	0.88	24.60	0.056	0.99	41.67	1.30 ×10 ⁻³
ZnO	40.10	0.71	51.95	0.057	0.96	43.47	5.57 ×10 ⁻⁴
BC	164.15	0.85	134.30	0.059	0.99	175.40	1.91 ×10 ⁻⁴
BZ	48.90	0.88	33.10	0.070	0.94	52.63	6.68 ×10 ⁻⁴
CZ	55.15	0.80	36.60	0.045	0.94	58.82	2.83 ×10 ⁻⁴
CZB	140.25	0.70	109.90	0.075	0.99	147.05	2.83 ×10 ⁻⁴

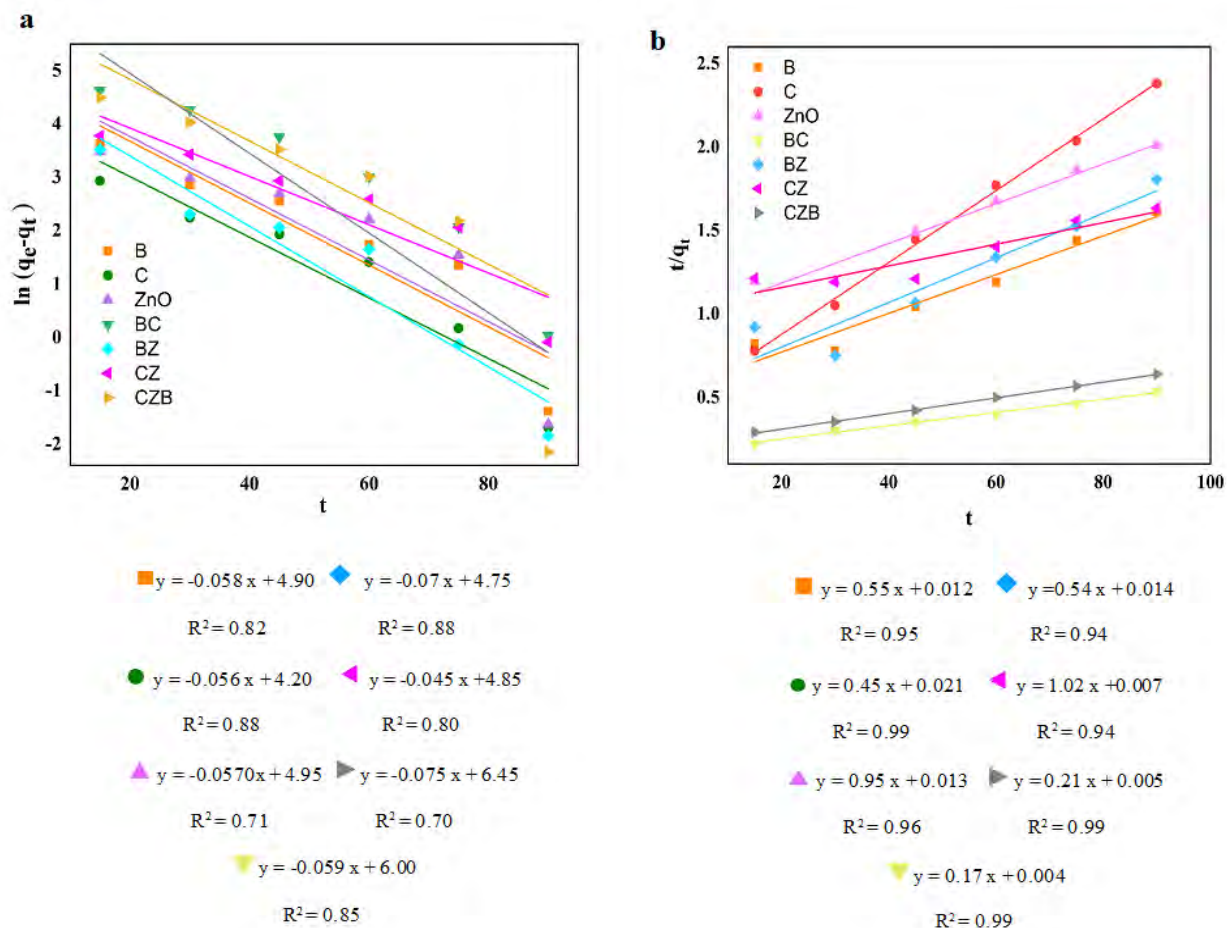


Fig 8. Linear fittings of pseudo-first (a) and pseudo-second (b) order kinetics.

4.4 Effect of Initial Concentration and Adsorption isotherms

When the initial dye concentration increased from 10 to 50mgL⁻¹, the adsorption was increased as shown in Fig.8. When further increasing the initial dye concentration in the range of 50–100mgL⁻¹, the adsorption of dye was slightly increased and the maximum dye adsorption occurred at equilibrium. When a low concentration of the dye solution was used, the number of active sites was sufficient for the removal of all dye molecules (Özdemir et al., 2015). This limited number of active sites was available for the definite number of the dye species in the solution (Chatterjee et al. 2005; Chiou and Li 2003).

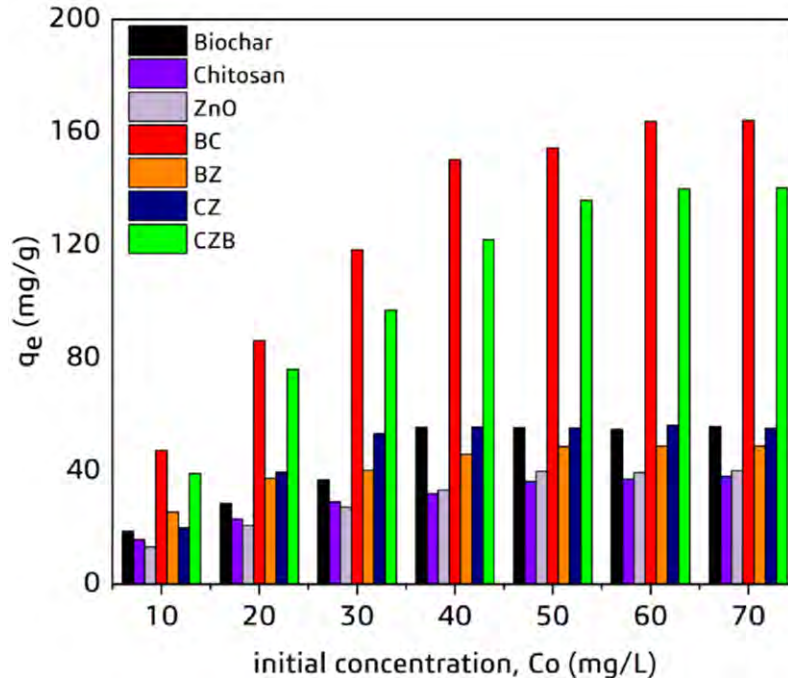


Fig. 9. Effect of concentration on adsorption of MB by Biochar (black), Chitosan (purple), ZnO (light purple), BC (red), BZ (orange), CZ (blue) and CZB (green)

The isotherm plots are presented in Fig. 9 (a), (b), (c) and the parameters are summarized in Table 9. The linear distribution of Fig.9 (a) and Pearson's R^2 value indicated the suitability of the Langmuir isotherm over the Freundlich isotherm (Abd-Elhamid et al., 2020). The calculated q_m , value is in accordance with the $q_{e,exp}$, which confirms the applicability of the Langmuir model to explain the adsorption behavior of MB on the adsorbents. The oxygenated functional groups of the biochar surface might act as the basement for the monolayer adsorption of dye molecules and provide the homogenous distribution of enthalpy over the surface of the biochar. In addition, the intensity parameter, $1/n$ from the Freundlich model of the B, C, Z, BC, BZ, CZ, and CZB found about 0.533, 0.413, 0.561, 0.648, 0.262, 0.414, and 0.424, respectively where the value of n denotes the degree of heterogeneity on the surface of the adsorbent; if $1/n < 1$ the process is favorable for adsorption, so the adsorption process is favorable. The disorganized 3D carbon with multiple cracks may contribute to the heterogenetic characteristics of the prepared adsorbents.

Table 9. Isotherm modeling parameters were obtained for Langmuir, Freundlich, and Temkin Isotherms. BC stands for Biochar-chitosan, BZ stands for Biochar-ZnO, CZ stands for chitosan-ZnO and CZB stands for chitosan-ZnO/biochar. (Adopted from Roy et al., 2022b)

Adsorbents	Langmuir			Freundlich			Temkin		
	R ²	k _L (Lmg ⁻¹)	q _m (mgg ⁻¹)	R ²	k _F (mgg ⁻¹). (Lmg ⁻¹) ^{1/n}	1/n	R ²	b _T (Jmol ⁻¹)	K _T (dm ³ g ⁻¹)
Biochar	0.96	0.048	78.92	0.90	7.27	0.533	0.94	132.56	0.40
Chitosan	0.99	0.066	47.73	0.97	7.36	0.413	0.99	233.45	0.61
ZnO	0.98	0.036	60.27	0.96	4.41	0.561	0.98	177.41	0.31
BC	0.99	0.396	179.8	0.94	13.66	0.648	0.97	38.68	0.26
BZ	0.99	0.169	54.22	0.94	17.87	0.262	0.98	258.35	3.23
CZ	0.98	0.118	65.87	0.88	12.19	0.414	0.88	164.68	0.98
CZB	0.99	0.168	164.7	0.90	33.68	0.424	0.90	69.57	1.56

The RSM approach implemented batch runs of CCD model developed trials to evaluate the effects of independent factors on the response and outcomes, as well as the experimental parameters. Among the coded values (X₁, X₂, X₃) of the three key process parameters and the associated response variable, polynomial regression modeling was carried out, and the best-fitted

model equation was generated as follows: Regression equations for removal (%), obtained from response surface methodology are mentioned in Eqn. (16)

$$\text{Removal (\%)} = 2.35539 + 0.169778 * \text{Time} + 0.195053 * \text{Concentration} + 16.0196 * \text{pH} + -0.000172727 * \text{Time} * \text{Concentration} + 0.0159563 * \text{Time} * \text{pH} + -0.013375 * \text{Concentration} * \text{pH} + -0.00108993 * \text{Time}^2 + -0.00696375 * \text{Concentration}^2 + -0.886039 * \text{pH}^2$$

(16)

Table 10. The ANOVA analysis of quadratic polynomial model with coefficient of determination (R^2) value 0.9843 for removal (%). (Adopted from Roy et al., 2022a)

Run	Independent variables			Response values (Removal %)	
	Time (minutes)	Concentration (ppm)	pH	Experimental Value	Predicted Value
1	10	10	2	34.5	33.7
2	10	60	10	55.1	55.6
3	90	35	9	89.2	87.7
4	90	35	9	90.8	87.6
5	120	60	2	23.9	23.2
6	65	35	6	72.5	74.3
7	10	60	2	19.5	17.7
8	120	60	10	73.8	75.2
9	120	10	10	95.1	97.5
10	65	35	6	73.1	74.3
11	10	10	10	76.5	77.1
12	120	10	2	40.9	40.1
13	157.5	35	6	76.2	75.9
14	7.5	35	6	62.9	63.9
15	65	35	6	74.5	74.4

16	65	35	0.7	15.1	17.8
17	65	35	12.7	75.5	74.5
18	65	77	6	45.6	45.9
\19	65	35	6	74.5	74.3
20	65	9.5	6	81.1	79.5

Statistical analysis (ANOVA) results revealed that the experimental data could be represented well with a quadratic polynomial model with a coefficient of determination (R^2) value of 0.9843 for removal (%). (Table 10)

Table 11. The ANOVA analysis of the variance quadratic model for removal of the dye. (Adopted from Roy et al., 2022a)

Source	Sum of Squares	df	Mean Square	F-value	p-value	
Model	11237.67	9	1248.63	294.65	< 0.0001	significant
A-Time	468.24	1	468.24	110.49	< 0.0001	
B-Concentration	983.50	1	983.50	232.09	< 0.0001	
C-pH	7320.06	1	7320.06	1727.38	< 0.0001	
AB	0.4513	1	0.4513	0.1065	0.7509	
AC	100.63	1	100.63	23.75	0.0006	
BC	14.31	1	14.31	3.38	0.0960	
A ²	95.89	1	95.89	22.63	0.0008	
B ²	167.47	1	167.47	39.52	< 0.0001	
C ²	1987.01	1	1987.01	468.89	< 0.0001	
Residual	42.38	10	4.24			
Lack of Fit	38.03	6	6.34	5.83	0.0549	not significant
Pure Error	4.35	4	1.09			
Core Total	11280.05	19				

In Table 11, the model F-value of 294.65 indicates the statistical significance of the model for MB removal and signifies only a chance of 0.01% by which a model F-value larger than the optimized value could occur due to the noise. The adequate precision ratio was found to be 38.03 from this model, which indicates a proper signal where it quantifies the signal to noise ratio, whereas a ratio of >4 is acceptable. The lack of fit value is 5.83, which confirms the developed model for removal efficiency of CZB for MB was statistically justified due to the non-significant lack of fit that indicates the good predictability of the model by RSM. In the experiment, there was only a 5.83% chance that a significant lack-of-fit F-value could occur due to noise. The P-values <0.0001 indicate that model terms are significant, whereas the values greater than 0.1000 are usually considered non-significant.

Table 12. Regression coefficient values for removal (%). (Adopted from Roy et al., 2022a)

Regression coefficients	Removal (%)
Intercept	78.98
A-Time	2.74
B-Concentration	-3.72
C-pH	17.45
AB	1.04
AC	1.39
BC	-0.8375
A ²	-2.69
B ²	-5.94
C ²	-12.19
R ²	0.9843

In our study, proximity to unity R^2 demonstrates that the influence of contact time (X_1), dye concentration (X_2), and pH (X_3) on response variables could be adequately described through a quadratic polynomial model. The significance level for coefficients of the quadratic polynomial model was determined through analysis of variance (ANOVA). A smaller P-value and greater F-

value is the indication of a highly significant effect of any term on the response variable (Abdulhameed et al., 2019, Karri et al., 2018).

4.5 Response Surface Analysis for CZB

4.5.1 Effect of independent variables on a response variable (removal (%))

The plot for the interactive effect of pH and contact time on the removal (%) by the CZB composite is represented in Fig. 10(a); at lowest conc. level. Contact time exhibited a linear effect on removal (%), but a quadratic ($p < 0.001$) behavior was observed for pH.

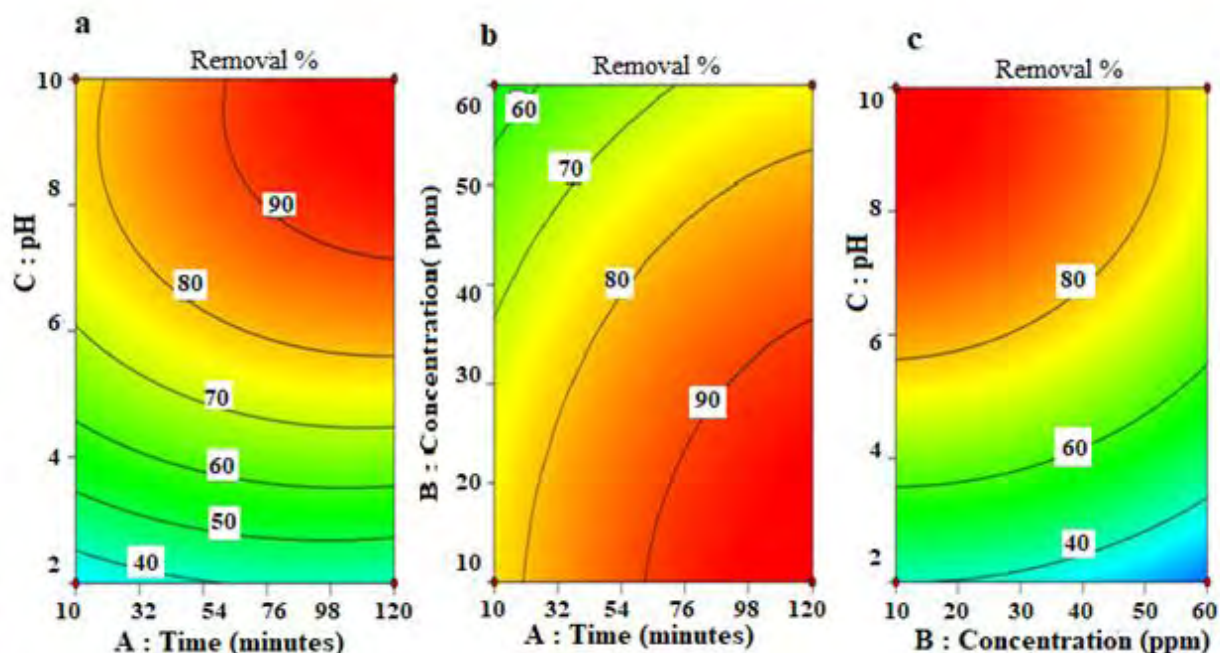


Fig. 10. Combined effects of pH and time (a), concentration and time (b) pH and concentration (c) on removal (%)

When the pH of the experiment solution is lower, there are a large number of protons (H^+) present in the solution. The opposite is true when the pH of the aqueous medium is raised, as there are significant amounts of OH^- groups in the solution. As a result, the adsorbent can provide more negative charges in an alkaline medium rather than an acidic medium, and because the dye's structure is cationic, removing the dye from the basic solution will be much easier. Consequently, at higher pH, due to a strong adsorbent-adsorbate interaction, an increase in removal (%) was seen

as the contact time was increased (Fig. 7). After a given amount of time has passed, the percentage of removal becomes constant. This may occur as a result of the saturation of the adsorbent's capturing sites over time. The combined effects of dye concentration and time on removal (%) are illustrated in Fig. 10(b); at highest pH level, which explicated the linear effect of both independent variables. At a constant dye concentration below around 60 ppm increase in removal (%) was observed with increasing contact time. At higher concentrations the removal (%) decreases due to the negative concentration gradient. At a certain level of time, the removal (%) became constant, further increase in time didn't enhance the removal (%) due to the saturation level of the adsorbent's capacity. Figure 10(c) represents the diagram for the combined effect of pH and initial dye concentration on the adsorptive behavior of MB onto the CZB. As the initial dye concentration increases up to a certain value with increasing pH, the removal percentage increases. However, after a certain value of concentration, removal (%) decreases for further increment in dye concentration at a constant pH. An increasing rate of dye uptake with increasing pH may be related to the opposite charges (negative) on the surface of the sorbent and on the dye molecules at higher pH. Similarly, decreasing removal (%) after crossing a certain concentration occurs due to the negative concentration gradient effect.

4.5.2 Optimization of independent variables and verification of RSM model

To illustrate the effects of contact time, concentration, and pH on removal (%), response surface graphs were drawn using design expert software. These graphs were generated by varying two independent variables within experimental ranges while keeping the third variable at the center point. Fig. 10 was generated by varying the contact time and pH at a central value of concentration at 50 mgL^{-1} , while by changing the concentration of dye and contact time at a central value of pH 6; whereas by changing the concentration of dye and pH at a central value of time at 65 min. These graphs illustrated complex interaction among independent variables. After that, numerical optimization was executed by desirability function using Design Expert Software. The goals selected for the optimization of removal (%) were within the range level of contact time, concentration, and pH in order to maximum removal (%). The solution with the maximum desirability value was selected as the optimized removal condition. Combined optimized were 49 min. contact time, 58 mgL^{-1} and 7.9 pH. The response value at optimized preparation conditions was 82.29 %. (Table 13).

Table 13. Optimum conditions and removal (%) at optimized condition

Optimum conditions	Values	
Time (minutes)	48.787	
Concentration (mg/L)	57.514	
pH	7.937	
Response	Predicted value	Actual value
Removal (%)	82.29	81.15

The validation of optimized preparation conditions was performed through experiments under optimized conditions. The response value at optimized preparation conditions was 82.29 %; whereas the experimental values at optimized preparation conditions were 81.15 %. The Experimental response value was well in agreement with predicted response values.

4.6 Response Surface Analysis for BC

4.6.1 The Model Fitting

To support the experimental result, response surface methodology (RSM) was utilized. It is both a logical and analytical strategy for optimizing the degree of independent variables. Table 14 presents the results of twenty experimental runs at different combinations of contact time (X_1), dye concentration (X_2) and pH (X_3). The effect of the independent variables on the removal (%) of MB by BC was clearly visible. The analysis of variance (ANOVA) revealed that the fit of the quadratic model (coefficient of determination, $R^2 = 0.99$) with experimental data was much better compared to linear ($R^2=0.61$), and 2FI ($R^2=0.58$) models. The R^2 of the quadratic model was close to unity which verifies that the effect of variables on %R would be adequately analyzed through a quadratic polynomial model. To estimate the values of the response variable, the coefficients of the polynomial equation were computed from obtained experimental data. The regression equation for removal (%), obtained from RSM is expressed in Eqn. (17).

$$\begin{aligned} \text{Removal (\%)} = & 6.58596 + 0.128066 * X_1 + 0.0507444 * X_2 + 17.1578 * X_3 + \\ & 5.45455e - 05 * X_1 * X_2 + 0.0197935 * X_1 * X_3 + -0.009 * X_2 * X_3 + \\ & -0.000902599 * X_1^2 + -0.00530844 * X_2^2 + -1.02372 * X_3^2 \end{aligned} \quad (17)$$

Table 14. Independent parameters and their corresponding levels for percentage removal (% R) for BC. (Adopted from Roy et al., 2022b)

Run	A: Time (minutes)	B: Concentration (ppm)	C: pH	Removal %
1	10	10	2	37.6
2	10	60	10	58.3
3	90	35	9	93.2
4	90	35	9	92.9
5	120	60	2	26.1
6	65	35	6	77.5
7	10	60	2	23.2
8	120	60	10	80.8
9	120	10	10	98.5
10	65	35	6	78.1
11	10	10	10	79.2
12	120	10	2	43.1
13	157.5	35	6	84.2
14	7.5	35	6	64.6
15	65	35	6	76.9
16	65	35	0.7	19.6
17	65	35	12.7	70.6
18	65	75	6	54.3
19	65	35	6	77.9
20	65	9.5	6	87.4

The significance levels for each coefficient of the derived model were determined through ANOVA and summarized in Table 15.

Table 15. The ANOVA analysis of the variance quadratic model for removal of the dye. (Adopted from Roy et al., 2022b)

Source	F-value	p-value	
Model	249.38	< 0.0001	significant
A-Time	115.40	< 0.0001	
B-Concentration	182.64	< 0.0001	
C-pH	1396.93	< 0.0001	
AB	0.0089	0.9266	
AC	30.71	0.0002	
BC	1.29	0.2834	
A ²	12.98	0.0048	
B ²	17.45	0.0019	
C ²	525.87	< 0.0001	
Residual			
Lack of Fit	37.32	0.0018	significant
Pure Error			
Cor Total			

The obtained model F-value was 249.38 with a p-value of <0.0001. This lower p-value justifies that, in this BC/dye system there is only a 0.01% chance that an F-value this large could occur due to noise (Abdulhameed et al.2019). In our case, considering high sensitivity, p-values less than 0.05 indicate model terms to be significant. In the BC/dye system, A, B, C, and C² were significant model terms. The adequate precision ratio was 52.80 (a ratio of >4 is acceptable), which indicates a proper signal-to-noise ratio. The lack of fit value for Eq. (17) was found to be 37.32, which validates the statistical justification of the developed model for BC due to the non-significant lack of fit. The reasonable predictability of the system by the RSM model was also justified. The lack

of fit p-value was 0.0018 (α), indicating only a 1.80% chance of a significant lack-of-fit F-value could occur due to noise in the experiment. The P-values <0.05 indicate that model terms are significant, whereas the values greater than 0.1000 are usually considered non-significant (Karri et al., 2018).

4.6.2 Effect of independent variables on a response variable (removal%)

The RSM obtained 3D surface graphs were utilized to analyze the MB sorption phenomenon by BC. The 3D graphs were generated by varying two independent variables (pH, time or pH, concentration or time, concentration) within the experimental ranges (Table 15) while keeping the third variable at the center point. The correlative representation of contact time, initial dye concentration, and pH on the removal (%) by BC is shown in Figure 11 (a, b, c). In Figure 9a, at a constant pH, lower removal was achieved with higher dye concentration. The increase in time increases the removal, which supports the analytical results. Table 15 shows each factor e.g., time, concentration and pH have a significant impact ($p < 0.0001$) on the removal. Figure 11 (b) presents the interactive relation of pH and contact time on the removal. At lower pH, there were abundantly available protons (H^+) in the system, that restricted the sorption of MB onto the oxygenated functional groups of BC (Cui et al., 2021). However, in an alkaline medium, the deprotonated functional groups interact with the MB molecules. After a certain time, removal reached a steady state, due to saturation of the active sites of BC over time. Figure 11 (c) presents the quadratic behavior of MB concentration and time on removal. At a constant dye concentration, an increase in removal was observed with increasing contact time. At higher concentrations, the removal decreases due to the negative concentration gradient. At a certain level of time, the removal reached a steady state and further increments in time caused zero impact on the removal (%) due to the saturation level of the BC capacity (Oyekanmi et al., 2021). Moreover, optimized preparation conditions were validated by performing experiments under optimized conditions. The response value at optimized preparation conditions was 83.1 %.

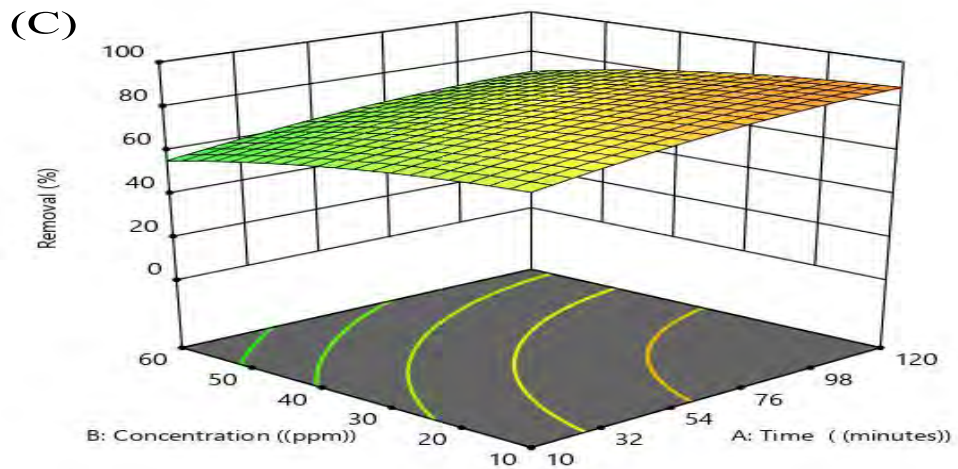
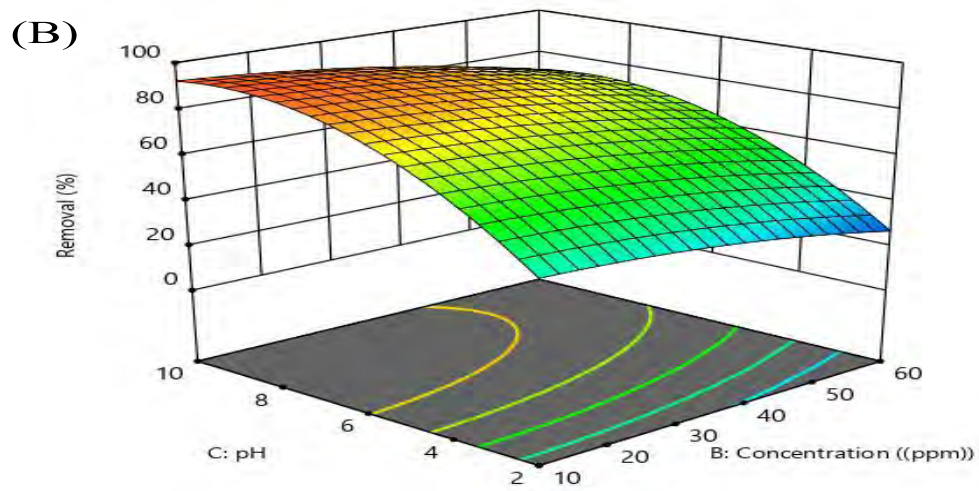
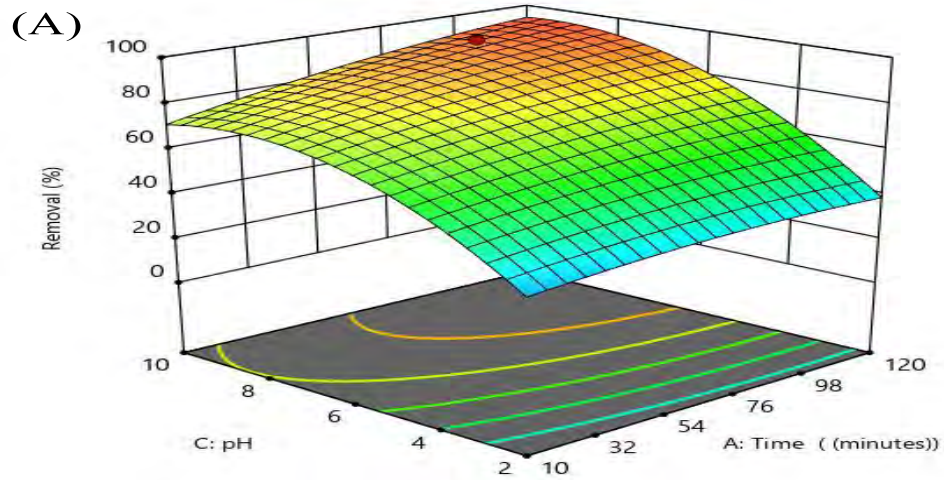


Fig. 11. Combined effects of pH and time (a), concentration and time (b) pH and concentration (c) on removal (%) for BC. (Adopted from Roy et al., 2022b)

4.7 Adsorption Mechanism

The mechanism of the adsorption process may vary depending on the adsorbent and adsorbate characteristics. The adsorption mechanisms; are basically a diffusion phenomenon through pores, hydrogen bonding, and π - π with π^+ - π interaction between the dye molecules and adsorbents (biochar, natural polymers, and metal oxides-based adsorbents). The porous diffusion consists of two distinct adsorption steps- the first step is the external diffusion of the dye molecules from the boundary layer to the surface of the components. This follows the internal diffusion in which the penetration of the dye molecules into the pores of the adsorbents occurs. As in the case of biochar-based materials; hydrogen bonding is favored in materials with oxygen-containing groups. Hydrogen bonding interaction may occur between the H-bonds (i.e., $-\text{COOH}$ or $-\text{OH}$ which act as the H-donors) on the adsorbent surface and the nitrogen in dyes (i.e., nitrogen atoms in the MB molecules, which act as the H-acceptors). The third one refers to a noncovalent interaction between π -acceptor and π -donor molecules, while π^+ - π (or cation- π interaction) is a noncovalent interaction between a surface of an aromatic π -donor and a cation. In π - π interaction, the aromatic rings in adsorbents act as π -electron donors and the aromatic rings in MB dye act as π -electron acceptors. Also, molecular structures of MB possess a cation N^+ , which may lead to the binding of cation N^+ to the π -face of aromatic rings in the adsorbent surface, forming π^+ - π interaction. The FTIR results of the materials revealed the presence of different functional groups in the BC and CZB composites. The XRD analysis indicated the stabilized crystallinity in the binary and ternary composites, whereas a fully amorphous structure of biochar was found. The SEM and EDS results revealed the highly porous structure of BZ and CZB composites. The BET surface area was highest for BZ and lowest for BC. However, the adsorption capacity was highest for BC following the CZB composite. The surface area is not the only factor that affects the adsorption capacity of an adsorbent but, in many cases the Point of Zero Charge (which changes with pH), the surface chemistry and the type of pores are factors driving the adsorption in a large extent. The removal is likely driven by the surface chemistry of the adsorbents. There would be a few possible mechanisms here: i. ion exchange/anchor if acidic functional groups are present/abundance, ii. C- π cation interaction if the surface is bold, or iii. combination of (i) and (ii). The very high surface area of any sorbent indicates the presence of narrow pores. These may be inaccessible for larger molecules of sorbate. A good indication of the functional groups present on the surface of adsorbents is the determination of the Point of Zero Charge. Depending on both, the working pH

in the solution and the pzc, whether the functional groups would be available to interact with the metal ions or not. The second point is porosity, the surface can be higher due to micropores but all of these micropores are not going to be useful to remove ions in the water phase. Variation of pore size causes the different types of affinity towards different adsorbates. Additionally, surface energy is considered another important factor for adsorption. For example, dispersive surface energy enhances the affinity towards non-polar molecules while specific surface energy becomes advantageous for polar molecules. As the adsorption results suggest that the lowest surface area resulted in the highest adsorption. So, surface area didn't play a major role in this phenomenon. The experimental results of pH effects show that adsorption of cationic MB dye was favored as pH increased. So, the major mode of adsorption of MB could be chemisorption due to an electrostatic interaction between the oxygenated functional groups and dye molecules.

CHAPTER 5

CONCLUSION AND FUTURE WORK

5.1 Conclusion

The following conclusions can be drawn from the study:

- i. The XRD results showed that the CZB composite is highly crystalline, and the average crystallite size of CZB nanocomposites was found to be 22.218 nm. It is evident that the presence of CZ as a stabilizer in biochar, reduced the crystallite size of CZB. All the diffraction peaks of CZB are in good agreement with those of the CZ structure. This, indeed, revealed that it is the successful formation of a nanosized CZB complex.
- ii. The SEM analysis showed that the surface morphology of biochar revealed the presence of macropores and irregular trough-like patterns, due to the decomposition and volatilization of raw materials. From the FESEM images of the CZ nanocomposite, it can be seen the particles appeared to be spherical in shape with quite distinct and uniform orientation.
- iii. From the SEM image the highest average particle size was found for BC about 35.74 nm and the lowest one for BZ about 19.43 nm. Besides, CZB has the lower average particle size of about 22.02 nm in comparison with CZ, i.e., 25.14 nm but higher than that of BZ, i.e., 19.43 nm respectively.
- iv. From the EDS results of CZ, the presence of Zn is observed. After the addition of CZ composite into biochar, it was observed that the porous and irregular shape of biochar converted into agglomerated form. It is due to the addition of CZ produced larger chunks and chunks of porous rock formed and agglomeration occurs between ZnO with chitosan.
- v. The highest adsorption capacity was observed for BZ composite (179.8 mg dyeg⁻¹) followed by CZB (164.7 mg dyeg⁻¹), biochar (78.9 mg dyeg⁻¹), CZ (65.87 mg dyeg⁻¹), ZnO (60.27 mg dyeg⁻¹), BZ (54.22 mg dyeg⁻¹) and Chitosan (47.73 mg dyeg⁻¹).
- vi. From the RSM model the response values at optimized preparation conditions for CZB and BC were 82.29 % and 83.1% respectively.

5.2 Future Scope of Works

The possible future works which can be suggested from the current study are listed below:

- i. The performance study of the synthesized biosorbent can be implemented for the actual textile wastewater treatment. This will give comprehensive knowledge about the possibility of industrial application.
- ii. Optimization of experimental parameters like changing pH and dye concentrations is necessary to obtain enhanced performance of the synthesized adsorbents due to the sensitivity of adsorption to the experimental parameters.
- iii. The recyclability and enhancement of the productive life cycle of adsorbents are the major limitations of the current process.

REFERENCES

REFERENCES

- Abidi, N., Duplay, J., Kleitz, C., Ceccantini, J., Jada, A., and Trabelsi-Ayadi, M., “The Application of Natural Clay Adsorbents for the Removal of Reactive Red 120 Dye from the Industrial Textile Effluents: Modelling, Kinetics and Thermodynamic Study,” *Journal of Colloid Science and Biotechnology*, vol. 5(2), pp. 145–156, 2016.
- AbdElhady, M. M., “Preparation and Characterization of Chitosan/Zinc Oxide Nanoparticles for Imparting Antimicrobial and UV Protection to Cotton Fabric,” *International Journal of Carbohydrate Chemistry*, vol. 2012, pp. 1–6, 2012.
- Abdulhameed, A. S., Jawad, A. H., and Mohammad, A. T., “Synthesis of chitosan-ethylene glycol diglycidyl ether/TiO₂ nanoparticles for adsorption of reactive orange 16 dye using a response surface methodology approach,” *Bioresource Technology*, vol. 293, pp. 122071, 2019.
- Afroze, S., Sen, T. K., Ang, M., and Nishioka, H. “Adsorption of methylene blue dye from aqueous solution by novel biomass Eucalyptus sheathiana bark: equilibrium, kinetics, thermodynamics and mechanism,” *Desalination and water treatment*, vol. 57(13), pp. 5858-5878, 2016.
- Ahmad, M., Yousaf, M., Nasir, A., Bhatti, I. A., Mahmood, A., Fang, X., Jian, X., Kalantar-Zadeh, K., and Mahmood, N., “Porous Eleocharis@MnPE Layered Hybrid for Synergistic Adsorption and Catalytic Biodegradation of Toxic Azo Dyes from Industrial Wastewater,” *Environmental Science & Technology*, vol. 53(4), pp. 2161–2170, 2019.
- Akter, S., and Islam, M. S., “Effect of Additional Fe²⁺ Salt on Electrocoagulation Process for the Degradation of Methyl Orange Dye: An Optimization and Kinetic Study,” *Heliyon*, vol. 8(8), pp. 10176, 2022.
- Akter, S., Suhan, M.B.K, and Islam, M. S., “Recent advances and perspective of electrocoagulation in the treatment of wastewater: A review,” *Environmental Nanotechnology, Monitoring & Management*, vol. 17, pp. 100643, 2022a.
- Akter, S., Islam M. S., Kabir, M. H., Shaikh, M. A. A., and Gafur, M. A., “UV/TiO₂ photodegradation of metronidazole, ciprofloxacin and sulfamethoxazole in aqueous solution: An optimization and kinetic study,” *Arabian Journal of Chemistry*, vol. 15 (7), pp. 103900, 2022b.

Al-Mamun, M. R., Kader, S., Islam, M. S., and Khan, M.Z.H., “Photocatalytic Activity improvement and application of UV-TiO₂ photocatalysis in textile wastewater treatment: a review,” *Journal of Environmental Chemical Engineering*, vol. 7(5), pp. 103248, 2019.

Al-Mamun, M. R., Islam, M. S., Hossain, M. R., Kader, S., Islam, M. S., and Khan, M.Z.H., “A novel and highly efficient Ag and GO co-synthesized ZnO nano photocatalyst for methylene blue dye degradation under UV irradiation,” *Environmental Nanotechnology, Monitoring & Management*, vol. 16, pp. 100495, 2021a.

Al-Mamun, M. R., Kader, S., and Islam, M. S., “Solar-TiO₂ immobilized photocatalytic reactors performance assessment in the degradation of methyl orange dye in aqueous solution,” *Environmental Nanotechnology, Monitoring & Management*, vol. 16, pp. 100514, 2021b.

Al-Ghouti, M. A., and Al-Absi, R. S., “Mechanistic understanding of the adsorption and thermodynamic aspects of cationic methylene blue dye onto cellulosic olive stones biomass from wastewater,” *Scientific Reports*, vol. 10(1), 2020.

Ali, S., Abbas, Y., Zuhra, Z., and Butler, I. S., “Synthesis of γ -alumina (Al₂O₃) nanoparticles and their potential for use as an adsorbent in the removal of methylene blue dye from industrial wastewater,” *Nanoscale Advances*, vol. 1, pp. 213-218, 2019.

Amode, J. O., Santos, J. H., Md. Alam, Z., Mirza, A. H., and Mei, C. C., “Adsorption of methylene blue from aqueous solution using untreated and treated (Metroxylon spp.) waste adsorbent: equilibrium and kinetics studies,” *International Journal of Industrial Chemistry*, vol. 7(3), pp. 333–345, 2016.

Amar, M. B., Walha, K., and Salvadó, V., “Valorisation of Pine Cone as an Efficient Biosorbent for the Removal of Pb(II), Cd(II), Cu(II), and Cr(VI),” *Adsorption Science & Technology*, vol. 2021, pp. 1–12, 2021.

Anil, I., Gunday, S. T., Bozkurt, A., and Alagha, O., “Design of Crosslinked Hydrogels Comprising Poly (Vinylphosphonic Acid) and Bis[2-(Methacryloyloxy)Ethyl] Phosphate as an Efficient Adsorbent for Wastewater Dye Removal,” *Nanomaterials*, vol. 10(1), pp. 131, 2020.

Auta, M., and Hameed, B. “Modified mesoporous clay adsorbent for adsorption isotherm and kinetics of methylene blue,” *Chemical Engineering Journal*, vol. 198–199, pp. 219–227, 2012.

Ayisha Sidiqqa, M., and Priya, V., “Removal of yellow dye using composite bonded adsorbent developed using natural clay and activated carbon from sapindus seed,” *Biocatalysis and Agricultural Biotechnology*, vol. 33, pp. 101965, 2021.

Bagheri, A., Abu-Danso, E., Iqbal, J. and Bhatnagar, A., “Modified biochar from Moringa seed powder for the removal of diclofenac from aqueous solution,” *Environmental Science and Pollution Research*, vol. 27, pp. 7318-7327, 2020.

Banerjee, S., Dubey, S., Gautam, R. K., Chattopadhyaya, M. C., and Sharma, Y. C., “Adsorption characteristics of alumina nanoparticles for the removal of hazardous dye, Orange G from aqueous solutions,” *Arabian Journal of Chemistry*, vol. 12(8), p. 5339-5354, 2019.

Baptisttella, A. M. S., de Araujo, C. M. B., Fraga, T. J. M., de Paiva, T. M. N., de Abreu, C. A. M., and da Motta Sobrinho, M. A., “Removal of textile dyes by benefited marine shells wastes: From circular economy to multi-phenomenological modeling”, *Journal of Environmental Management*, vol. 296, pp. 113222, 2021.

Banerjee, S., and Chattopadhyaya, M., “Adsorption characteristics for the removal of a toxic dye, tartrazine from aqueous solutions by a low cost agricultural by-product,” *Arabian Journal of Chemistry*, vol. 10, pp. 1629–S1638, 2017.

Beil, S., Schamberger, A., Naumann, W., Machill, S., and Van Pée, K. H., “Determination of the degree of N-acetylation (DA) of chitin and chitosan in the presence of water by first derivative ATR FTIR spectroscopy,” *Carbohydrate polymers*, vol. 87(1), pp. 117-122, 2012.

Borys, P., and Grzywna, Z. J., “On the fractality of the Freundlich adsorption isotherm in equilibrium and non-equilibrium cases,” *Physical Chemistry Chemical Physics*, vol. 18(30), pp. 20784–20789, 2016.

Chai, W. S., Cheun, J. Y., Kumar, P. S., Mubashir, M., Majeed, Z., Banat, F., and Show, P. L., “A review on conventional and novel materials towards heavy metal adsorption in wastewater treatment application,” *Journal of Cleaner Production*, vol. 126589, 2021.

Chauhan, P. S., Kant, R., Rai, A., Gupta, A., and Bhattacharya, S., “Facile synthesis of ZnO/GO nanoflowers over Si substrate for improved photocatalytic decolorization of MB dye and industrial wastewater under solar irradiation,” *Materials Science in Semiconductor Processing*, vol. 89, pp. 6-17, 2019.

Chen, M., Bao, C., Hu, D., Jin, X., and Huang, Q., “Facile and low-cost fabrication of ZnO/biochar nanocomposites from jute fibers for efficient and stable photodegradation of methylene blue dye,” *Journal of Analytical and Applied Pyrolysis*, vol. 139, pp. 319–332, 2019.

Chenlu, J., Li, T., Wang, J., Wang, H., Zhang, X., Han, X., and Yuyue, C., “Efficient removal of dyes from aqueous solution by a porous sodium alginate/gelatin/graphene oxide triple-network composite aerogel,” *Journal of Polymers and the Environment*, vol. 28(5), pp. 1492-1502, 2020.

Clemente, J. S., Beauchemin, S., Thibault, Y., MacKinnon, T., and Smith, D., “Differentiating Inorganics in Biochars Produced at Commercial Scale Using Principal Component Analysis,” *ACS Omega*, vol. 3(6), pp. 6931–6944, 2018.

Choi, J., Islam, M. S., Tumpa, F., and Liu, Y., “Biological fixed film,” *Water Environment Research*, vol. 85 (10), pp. 1060-1091, 2013.

Crini, G., Lichtfouse, E., Wilson, L. D., and Morin-Crini, N., “Conventional and non-conventional adsorbents for wastewater treatment,” *Environmental Chemistry Letters*, vol. 17(1), pp. 195-213, 2019.

Cui, L., Fan, Q., Sun, J., Quan, G., Yan, J., Hina, K., Wang, H., Zhang, Z., and Hussain, Q., “Changes in surface characteristics and adsorption properties of 2,4,6-trichlorophenol following Fenton-like aging of biochar,” *Scientific Reports*, vol. 11(1). P. 4293, 2021.

Dalvand, A., Gholibegloo, E., Ganjali, M. R., Golchinpoor, N., Khazaei, M., Kamani, H., and Mahvi, A. H., “Comparison of Moringa stenopetala seed extract as a clean coagulant with Alum and Moringa stenopetala-Alum hybrid coagulant to remove direct dye from Textile Wastewater,” *Environmental Science and Pollution Research*, vol. 23(16), pp. 16396-16405, 2016.

Dongare, P. D., Alabastri, A., Pedersen, S., Zodrow, K. R., Hogan, N. J., Neumann, O., Wu, J., Wang, T., Deshmukh, A., Elimelech, M., Li, Q., Nordlander, P., and Halas, N. J., “Nanophotonics-enabled solar membrane distillation for off-grid water purification,” *Proceedings of the National Academy of Sciences*, vol. 114(27), pp. 6936–6941, 2017.

Dutta, S., Gupta, B., and Srivastava, S.K., “Recent advances on the removal of dyes from wastewater using various adsorbents: a critical review,” *Materials Advances*, vol. 2(14), p. 4497-4531, 2021.

Eddy, M., Tbib, B., and EL-Hami, K., “A comparison of chitosan properties after extraction from shrimp shells by diluted and concentrated acids,” *Heliyon*, vol. 6(2), pp. 03486, 2020.

Fan, M., Hu, Q., and Shen, K., “Preparation and structure of chitosan soluble in wide pH range,” *Carbohydrate Polymers*, vol. 78(1), pp. 66–71, 2009.

Fernandes Queiroz, M., Melo, K. R. T., Sabry, D. A., Sasaki, G. L., and Rocha, H. A. O., “Does the use of chitosan contribute to oxalate kidney stone formation?,” *Marine drugs*, vol. 13(1), pp. 141-158, 2015.

Foo, K. Y., and Hameed, B. H., “An overview of dye removal via activated carbon adsorption process,” *Desalination and Water Treatment*, vol. 19(1–3), pp. 255–274, 2010.

Foster, J. E., “Plasma-based water purification: Challenges and prospects for the future,” *Physics of Plasmas*, vol. 24(5), pp. 055501, 2017.

Geetha, M., Nagabhushana, H., and Shivananjaiah, H., “Green mediated synthesis and characterization of ZnO nanoparticles using Euphorbia Jatropa latex as reducing agent,” *Journal of Science: Advanced Materials and Devices*, vol. 1(3), pp. 301–310, 2016.

Gwenzi, W., Chaukura, N., Noubactep, C., and Mukome, F.N.D., “Biochar-based water treatment systems as a potential low-cost and sustainable technology for clean water provision,” *Journal of environmental management*, vol. 197, pp. 732–749, 2017.

Hassan, H., Salama, A., El-ziaty, A. K., and El-Sakhawy, M., “New chitosan/silica/zinc oxide nanocomposite as adsorbent for dye removal,” *International Journal of Biological Macromolecules*, vol. 131, pp. 520–526, 2019.

Harouna, M., Tcheka, C., and Dobe, N., “Batch Equilibrium and Kinetic Studies of Anionic and Cationic Dyes Adsorption onto Al–Pillared Clay from a Local Cameroonian Clay Materials in Aqueous Medium,” *Modern Chemistry*, vol. 8(2), pp. 23, 2020.

Hasanzadeh, M., Simchi, A., and Far, H. S., “Nanoporous composites of activated carbon-metal organic frameworks for organic dye adsorption: Synthesis, adsorption mechanism and kinetics studies,” *Journal of Industrial and Engineering Chemistry*, vol. 81, pp. 405-414, 2020.

Hu, C., Lu, L., Zhu, Y., Li, R., and Xing, Y., “Morphological controlled preparation and photocatalytic activity of zinc oxide,” *Materials Chemistry and Physics*, vol. 217, pp. 182–191, 2018.

Herrera-González, A.M., M. Caldera-Villalobos, and A.-A. Peláez-Cid, “Adsorption of textile dyes using an activated carbon and crosslinked polyvinyl phosphonic acid composite,” *Journal of Environmental Management*, vol. 234, p. 237-244, 2019.

Hussain, I., Li, Y., Qi, J., Li, J., and Wang, L., “Nitrogen-enriched carbon sheet for Methyl blue dye adsorption,” *Journal of Environmental Management*, vol. 215, pp. 123–131, 2018.

Hwang, G., Dong, T., Islam, M. S., Sheng, Z. Y., Perez-Estrada, L. A., Liu, Y., and Gamal El-Din, M., “The impacts of ozonation on oil sands process-affected water biodegradability and biofilm formation characteristics in bioreactors,” *Bioresource Technology*, vol. 130, pp. 269-277, 2013.

Inam, E., Etim, U., Akpabio, E., and Umoren, S., “Process optimization for the application of carbon from plantain peels in dye abstraction,” *Journal of Taibah University for Science*, vol. 11(1), pp. 173–185, 2017.

Ikram, R., Jan, B. M., and Ahmad, W., “Advances in synthesis of graphene derivatives using industrial wastes precursors; prospects and challenges,” *Journal of Materials Research and Technology*, vol. 9(6), pp. 15924-15951, 2020.

Islam, M. S., Hwang, G. Liu, Y., Biological fixed film. *Water Environment Research. Literature Review*, vol. 84 (10), pp. 1081-1113, 2012.

Islam, M. S. Dong, T., McPhedran, K. N., Sheng, Z., Zhang, Y., Liu, Y., and Gamal El-Din, M., Impact of ozonation pre-treatment of oil sands process-affected water on the operational performance of a GAC-fluidized bed biofilm reactor,” *Biodegradation*, vol. 25(6), pp. 811-823, 2014a.

Islam, M. S. Dong, T., Sheng, Z., Zhang, Y., Liu, Y., and Gamal El-Din, M., “Microbial community structure and operational performance of a fluidized bed biofilm reactor treating oil sands process-affected water,” *International Biodeterioration and Biodegradation*, vol. 91, pp. 111–118, 2014b.

Islam, M. S., Tumpa, F., Xue, J. Kai, C. Liu, Sharma, K., and Shi, Y., Y., “Biological fixed film. *Water Environment Research*, vol. 86(10), pp. 1070-1100, 2014c.

Islam, M.S., Zhang, Y., McPhedran, K.N., Liu, Y., and Gamal El-Din, M., “Granular activated carbon for simultaneous adsorption and biodegradation of toxic oil sands process-affected water organic compounds,” *Journal of Environmental Management*, vol. 152, pp. 49-57, 2015a.

Islam, M. S. Zhang, Y., McPhedran, K. N., and Liu, Y., “Gamal El-Din, M., Next-Generation Pyrosequencing Analysis of Microbial Biofilm Communities on Granular Activated Carbon in Treatment of Oil Sands Process-Affected Water,” *Applied and Environmental Microbiology*, vol. 81(12), pp. 4037-4048, 2015b.

Dong, T., Zhang, Y., Islam, M. S., Liu, Y., Gamal El-Din, M., “The impact of various ozone pre-treatment doses on the performance of endogenous microbial communities for the remediation of

oil sands process-affected water”, *International Biodeterioration and biodegradation*, vol.100, pp. 17-28, 2015c.

Islam, M. S., Zhang, Y., Dong, S. McPhedran, K. N., Rashed, E. M., El-Shafei, M. M., Noureldin, A. M., and Gamal El-Din, M., “Dynamics of microbial community structure and nutrient removal from an innovative side-stream enhanced biological phosphorus removal process,” *Journal of Environmental Management*, vol. 198, (1), pp. 300-307, 2017.

Islam, M.S., McPhedran, K.N., Messele, S.A., Liu, Y., and Gamal El-Din, M., “Isotherm and kinetic studies on adsorption of oil sands process-affected water organic compounds using granular activated carbon,” *Chemosphere* vol. 202, pp. 716-725, 2018.

Islam, M., S., Kwak, J-H., Nzediegwu, C., Wang, S., Palansuriya, K., Kwon, E., E., Anne Naeth, M., Gamal El-Din, M., Ok, Y., S., and Chang, S. X., “Biochar heavy metal removal in aqueous solution depends on feedstock type and pyrolysis purging gas”, *Environmental Pollution*, vol. 281, pp. 117094, 2021a.

Islam, M. S., Sanzida, N., Rahman, M., R., and Alam, D. M., “From the value chain to environmental management of used lube oil: A baseline study in Bangladesh,” *Case Studies in Chemical and Environmental Engineering*, vol. 4, pp. 100159, 2021b.

Islam, M.S., Roy, H., and Afrose, S., “Phosphoric Acid Surface Modified Moringa oleifera Leaves Biochar for the Sequestration of Methyl Orange from Aqueous Solution: Characterizations, Isotherm and Kinetics Analysis,” *Remediation*, vol. 32(4), pp. 281-298, 2022.

Islam, M., T., Jahan, T., and Islam., M.S., “A study on the efficiency of fatted and defatted Moringa oleifera seed extract (MOSE) on indigo carmine dye removal,” *Journal of Functional Materials and Chemical Engineering*, vol. 1(1), pp. 97-102, 2019.

Islam, M. S. Zhang, Y., McPhedran, K. N., Liu, Y., and Gamal El-Din, M., “Mechanistic investigation of industrial wastewater naphthenic acids removal using granular activated carbon (GAC) biofilm based processes,” *Science of the Total Environment*. Vol. 541, pp. 238-246, 2016.

Ismail, M., Akhtar, K., Khan, M., Kamal, T., Khan, M. A., M. Asiri, A., Seo, J., and Khan, S. B., “Pollution, Toxicity and Carcinogenicity of Organic Dyes and their Catalytic Bio-Remediation,” *Current Pharmaceutical Design*, vol. 25(34), pp. 3645–3663, 2019.

Jahan, N., Roy, H., Reaz, A.H., Arshi, S., Rahman, E., Firoz, S.H., and Islam, M.S., “A comparative study on sorption behavior of graphene oxide and reduced graphene oxide towards

methylene blue,” *Case Studies in Chemical and Environmental Engineering*, vol. 6, pp. 100239. 2022.

Jan, H., Shah, M., Usman, H., Khan, M. A., Zia, M., Hano, C., and Abbasi, B. H., “Biogenic Synthesis and Characterization of Antimicrobial and Antiparasitic Zinc Oxide (ZnO) Nanoparticles Using Aqueous Extracts of the Himalayan Columbine (*Aquilegia pubiflora*),” *Frontiers in Materials*, vol. 7, 2020.

Janu, R., Mrlik, V., Ribitsch, D., Hofman, J., Sedláček, P., Bielská, L., and Soja, G., “Biochar surface functional groups as affected by biomass feedstock, biochar composition and pyrolysis temperature,” *Carbon Resources Conversion*, vol. 4, pp. 36–46, 2021.

Khandelwal, N., Tiwari, E., Singh, N., Marsac, R., Schäfer, T., Monikh, F. A., and Darbha, G. K., “Impact of long-term storage of various redox-sensitive supported nanocomposites on their application in removal of dyes from wastewater: Mechanisms delineation through spectroscopic investigations,” *Journal of Hazardous Materials*, vol. 401, pp. 123375, 2021.

Kader, S., Al- Mamun M.R., Suhan, M.B.K., Shuchi, S.B., and Islam M.S., “Enhanced photodegradation of methyl orange dye under UV irradiation using MoO₃ and Ag doped TiO₂ photocatalysts,” *Environmental Technology & Innovation*, vol. 17, pp. 102476, 2022.

Kamaraj, M., Srinivasan, N., Assefa, G., Adugna, A. T., and Kebede, M., “Facile development of sunlit ZnO nanoparticles-activated carbon hybrid from pernicious weed as an operative nano-adsorbent for removal of methylene blue and chromium from aqueous solution: Extended application in tannery industrial wastewater,” *Environmental Technology & Innovation*, vol. 17, pp. 100540, 2020.

Kannaujiya, MC., Mandal, T., Mandal, DD., and Mondal, MK., “Treatment of Leather Industry Wastewater and Recovery of Valuable Substances to Solve Waste Management Problem in Environment, Environmental Contaminants: Ecological Implications and Management,” *Springer*, pp. 311-340, 2019.

Karri, R. R., Tanzifi, M., Tavakkoli Yaraki, M., and Sahu, J., “Optimization and modeling of methyl orange adsorption onto polyaniline nano-adsorbent through response surface methodology and differential evolution embedded neural network,” *Journal of Environmental Management*, vol. 223, pp. 517–529, 2018.

- Kefeni, K. K., and Mamba, B. B., “Photocatalytic application of spinel ferrite nanoparticles and nanocomposites in wastewater treatment: Review,” *Sustainable Materials and Technologies*, vol. 23, pp. 00140, 2020.
- Khan, M. M. U. R., “Analytical Solution of Van Der Pol’s Differential Equation Using Homotopy Perturbation Method,” *Journal of Applied Mathematics and Physics*, vol.07(01), pp.1–12, 2019.
- Khamizov, R. K., “A Pseudo-Second Order Kinetic Equation for Sorption Processes,” *Russian Journal of Physical Chemistry A*, vol. 94(1), pp. 171–176, 2020.
- Kumar, S., Mukherjee, S., Kr. Singh, R., Chatterjee, S., and Ghosh, A. K., “Structural and optical properties of sol-gel derived nanocrystalline Fe-doped ZnO,” *Journal of Applied Physics*, vol. 110(10), pp. 103508, 2011.
- Kougias, D. G., “Herbicide biomonitoring in agricultural workers in Valle del Mayo, Sonora Mexico,” *Environmental Science and Pollution Research*,” vol. 27(14), pp. 17429–17433, 2020.
- Kwak, J., Islam, M. S., Wang, S., Messele, S.A., Naeth, M. A., Gamal El-Din, M., and Chang, S. X., “Biochar properties and lead(II) adsorption capacity depend on feedstock type, pyrolysis temperature, and steam activation,” *Chemosphere*, vol. 31, pp. 393-404, 2019.
- Kumari, P., Sharma, P., Srivastava, S., and Srivastava, M. M., “Biosorption studies on shelled Moringa oleifera Lamarck seed powder: Removal and recovery of arsenic from aqueous system,” *International Journal of Mineral Processing*, vol. 78, pp. 131-139, 2006.
- Li, L., Chen, Q., Zhao, C., Guo, B., Xu, X., Liu, T., and Zhao, L., “A novel chitosan modified magnesium impregnated corn straw biochar for ammonium and phosphate removal from simulated livestock wastewater,” *Environmental Technology & Innovation*, vol. 26, pp. 102519, 2022.
- Liu, S., Ma, C., Ma, M-G., and Xu, F., “Magnetic Nanocomposite Adsorbents, Composite Nano-adsorbents,” *Elsevier*, pp. 295-316, 2019.
- Liu, Q., Zhou, Y., Lu, J., and Zhou, Y., “Novel cyclodextrin-based adsorbents for removing pollutants from wastewater: A critical review,” *Chemosphere*, vol. 241, pp. 125043, 2020.
- Liu, L., Luo, X. B., Ding, L., and Luo, S. L., “Application of Nanotechnology in the Removal of Heavy Metal From Water,” *Nanomaterials for the Removal of Pollutants and Resource Reutilization*, pp. 83–147, 2019.
- Lin, S. H., and Juang, R. S., “Adsorption of phenol and its derivatives from water using synthetic resins and low-cost natural adsorbents: A review,” *Journal of Environmental Management*, vol. 90(3), pp. 1336–1349, 2009.

Mostafa, M. H., Elsayy, M. A., Darwish, M. S., Hussein, L. I., and Abdaleem, A. H., "Microwave-Assisted preparation of Chitosan/ZnO nanocomposite and its application in dye removal," *Materials Chemistry and Physics*, vol. 248, pp. 122914, 2020.

Machineni, L., "Review on biological wastewater treatment and resources recovery: attached and suspended growth systems," *Water Science and Technology*, vol.80(11), pp.2013-2026, 2020.

Mashkoo, F., and Nasar, A., "Mag Sorbents: Potential candidates in wastewater treatment technology—A review on the removal of methylene blue dye," *Journal of magnetism and magnetic materials*, vol. 500, pp. 166408, 2020.

Mazumder, P., PM, A., Jyoti, Khwairakpam, M., Mishra, U., and Kalamdhad, A. S., "Enhancement of soil physico-chemical properties post compost application: Optimization using Response Surface Methodology comprehending Central Composite Design," *Journal of Environmental Management*, vol. 289, pp. 112461, 2021.

Mohan, D., Kumar, A., and Pittman, C. U., "Sustainable biochar-a tool for climate change mitigation, soil management and water and wastewater treatment in Geostatistical and Geospatial Approaches for the Characterization of Natural Resources in the Environment," *Springer, Cham*, pp. 949-952, 2016.

Mohamed, R. M., and Ismail, A. A., "Mesoporous BiVO₄/2D-g-C₃N₄ heterostructures for superior visible light-driven photocatalytic reduction of Hg(II) ions," *Ceramics International*, vol. 47(18), pp. 26063–26073, 2021.

Mukherjee, A., Zimmerman, A., and Harris, W., "Surface chemistry variations among a series of laboratory-produced biochars," *Geoderma*, vol. 163(3–4), pp. 247–255, 2011.

Niasar, H. S., Das, S., Xu, C. C., and Ray, M. B., "Continuous column adsorption of naphthenic acids from synthetic and real oil sands process-affected water (OSPW) using carbon-based adsorbents," *Chemosphere*, vol. 214, pp. 511–518, 2019.

Nanjani, S., and Keharia, H. K., "Alterations in Microbial Community Structure and Function in Response to Azo Dyes," In *Microbiome-Host Interactions*, pp. 367-395, 2021.

Nartey, O. D., and Zhao, B., "Biochar Preparation, Characterization, and Adsorptive Capacity and Its Effect on Bioavailability of Contaminants: An Overview," *Advances in Materials Science and Engineering*, vol. 2014, pp. 1–12, 2014.

- Nguyen, N. T., Nguyen, N. T., and Nguyen, V. A., “In Situ Synthesis and Characterization of ZnO/Chitosan Nanocomposite as an Adsorbent for Removal of Congo Red from Aqueous Solution,” *Advances in Polymer Technology*, vol. 2020, pp. 1–8, 2020.
- Özdemir, M., Durmuş, Z., ŞAhin, M., & Saka, C., “Removal of methylene blue, methyl violet, rhodamine B, alizarin red, and bromocresol green dyes from aqueous solutions on activated cotton stalks,” *Desalination and Water Treatment*, vol. 57(38), pp. 18038–18048, 2015.
- Oyekanmi, A. A., Ahmad, A., Mohd Setapar, S. H., Alshammari, M. B., Jawaid, M., Hanafiah, M. M., Abdul Khalil, H. P. S., and Vaseashta, A., “Sustainable Durio zibethinus-Derived Biosorbents for Congo Red Removal from Aqueous Solution: Statistical Optimization, Isotherms and Mechanism Studies.” *Sustainability*, vol.13(23), pp.13264, 2021.
- Pandiyarajan, T., and Karthikeyan, B., “Optical properties of annealing induced post growth ZnO: ZnFe₂O₄ nanocomposites,” *Spectrochimica Acta Part A: Molecular and Biomolecular Spectroscopy*, vol. 106, pp. 247-252, 2013.
- Pan, X., Gu, Z., Chen, W., and Li, Q., “Preparation of biochar and biochar composites and their application in a Fenton-like process for wastewater decontamination: A review,” *Science of The Total Environment*, vol. 754, pp. 142104, 2021.
- Peña-Guzmán, C., Ulloa-Sánchez, S., Mora, K., Helena-Bustos, R., Lopez-Barrera, E., Alvarez, J., and Rodríguez-Pinzón, M., “Emerging pollutants in the urban water cycle in Latin America: A review of the current literature,” *Journal of environmental management*, vol. 237, pp. 408-423, 2019.
- Patawat, C., Silakate, K., Chuan-udom, S., and Supanchaiyamat, N., “Preparation of activated carbon from Dipterocarpus alatus fruit and its application for methylene blue adsorption,” *RSC Advances*, vol. 10(36), pp. 21082-21091, 2020.
- Petrovic, B., Gorbounov, M., and Masoudi Soltani, S., “Impact of Surface Functional Groups and Their Introduction Methods on the Mechanisms of CO₂ Adsorption on Porous Carbonaceous Adsorbents,” *Carbon Capture Science & Technology*, vol. 3, pp. 100045, 2022.
- Plazinski, W., Rudzinski, W., and Plazinska, A., “Theoretical models of sorption kinetics including a surface reaction mechanism: A review,” *Advances in Colloid and Interface Science*, vol. 152(1–2), pp. 2–13, 2009.

- Prajapati, A. K., and Mondal, M. K., “Hazardous As(III) removal using nanoporous activated carbon of waste garlic stem as adsorbent: Kinetic and mass transfer mechanisms,” *Korean Journal of Chemical Engineering*, vol. 36(11), pp. 1900–1914, 2019.
- Pereira, A. S., Islam, M. S., Gamal El-Din, M., and Martin, J. W., “Ozonation degrades all detectable organic compound classes in oil sands process-affected water; an application of high-performance liquid chromatography/orbitrap mass spectrometry,” *Rapid Communications in Mass Spectrometry*, vol. 27, pp. 2317-2326, 2013.
- Pourrezaei, P., Afzal, A., Ding, N., Islam, M. S., Moustafa, A., Drzewicz, P., Chelme-Ayala, P., and Gamal El-Din, M., “Physico-chemical processes,” *Water Environment Research Literature Review*, vol. 82(10), pp. 997-1072, 2010.
- Rashid, R., Shafiq, I., Akhter, P., Iqbal, M. J., and Hussain, M., “A state-of-the-art review on wastewater treatment techniques: the effectiveness of adsorption method,” *Environmental Science and Pollution Research*, vol. 28(8), pp. 9050–9066, 2021.
- Rattanapan, S., Srikram, J., and Kongsune, P., “Adsorption of Methyl Orange on Coffee grounds Activated Carbon,” *Energy Procedia*, vol. 138, pp. 949–954, 2017.
- Rendo, D., “Adsorption of Methylene Blue Dye using Fe₃O₄ Magnetized Natural Zeolite Adsorbent,” *Jurnal Kimia Sains Dan Aplikasi*, vol. 24(2), pp. 51–57, 2021.
- Rosales, E., Mejjide, J., Pazos, M., and Sanromán, M. A., “Challenges and recent advances in biochar as low-cost biosorbent: From batch assays to continuous-flow systems,” *Bioresource Technology*, vol. 246, pp. 176–192, 2017.
- Roy, H., Prantika, T. R., Riyad, M., Paul, S., and Islam, M.S., “Synthesis, characterizations, and RSM analysis of Citrus macroptera peel derived biochar for textile dye treatment,” *South African Journal of Chemical Engineering*, vol. 41, pp. 129–139, 2022.
- Roy, H., Islam, M. S., Arifin, M. T., & Firoz, S. H., “Chitosan-ZnO decorated Moringa oleifera seed biochar for sequestration of methylene blue: Isotherms, kinetics, and response surface analysis,” *Environmental Nanotechnology, Monitoring & Management*, vol. 18, pp. 100752, 2022a.
- Roy, H., Islam, M. S., Arifin, M. T., and Firoz, S. H., “Synthesis, Characterization and Sorption Properties of Biochar, Chitosan and ZnO-Based Binary Composites towards a Cationic Dye,” *Sustainability*, vol. 14(21), pp. 14571, 2022b.

Sabouni, R., Aidan, A., AlObeidli, A., Lahib, F., Bacha, H. H., Kassermally, R., and Jarmakani, S., "Adsorption kinetics and thermodynamics of Methylene Blue by HKUST-1," *Desalination and Water Treatment*, vol. 138, pp. 301–312, 2019.

Saini, K. and Malhotra S., "Environmental Pollution," *International Journal of Engineering Research and Applications*, vol. 6(6), 2016.

Sahnoun, S., Boutahala, M., Tiar, C., and Kahoul, A., "Adsorption of tartrazine from an aqueous solution by octadecyl trimethylammonium bromide-modified bentonite: Kinetics and isotherm modeling," *Comptes Rendus Chimie*, vol. 21(3–4), pp. 391–398, 2018.

Samsami, S., Mohamadi, M., Sarrafzadeh, M.H., Rene, E.R., and Firoozbahr, M., "Recent advances in the treatment of dye-containing wastewater from textile industries: Overview and perspectives," *Process Safety and Environmental Protection*, vol. 143, pp. 138-163, 2020.

Saravanan, A., Kumar, P. S., Yaashikaa, P. R., Kanmani, S., Varthine, R. H., Muthu, C. M. M., & Yuvaraj, D., "Modelling on the removal of dye from industrial wastewater using surface improved *Enteromorpha intestinalis*," *International Journal of Environmental Research*, vol. 13(2), pp. 349-366, 2019.

Saxena, M., Sharma, N., and Saxena, R., "Highly efficient and rapid removal of a toxic dye: Adsorption kinetics, isotherm, and mechanism studies on functionalized multiwalled carbon nanotubes," *Surfaces and Interfaces*, vol. 21, pp. 100639, 2020.

Seiwert, B., and Reemtsma, T., "Hexamethoxymethylmelamine—a precursor of persistent and mobile contaminants in municipal wastewater and the water cycle," *Water research*, vol. 165, pp. 114973, 2019.

Sewu, D. D., Jung, H., Kim, S. S., Lee, D. S., and Woo, S. H., "Decolorization of cationic and anionic dye-laden wastewater by steam-activated biochar produced at an industrial-scale from spent mushroom substrate," *Bioresource Technology*, vol. 277, pp. 77–86, 2019.

Shafiq, I., Hussain, M., Shehzad, N., Maafa, I. M., Akhter, P., Amjad, U. E. S., Shafique, S., Razzaq, A., Yang, W., Tahir, M., and Russo, N., "The effect of crystal facets and induced porosity on the performance of monoclinic BiVO₄ for the enhanced visible-light driven photocatalytic abatement of methylene blue," *Journal of Environmental Chemical Engineering*, vol. 7(4), pp. 103265, 2019.

Shuchi, S. B., Suhan, M. B. K., Humayun, S. B., Haque, M. E., and Islam, M. S., "Heat-activated potassium persulfate treatment of Sudan Black B dye: Degradation kinetic and thermodynamic studies," *Journal of Water Process Engineering*, vol. 39, pp. 101690, 2021.

Sackey, E. A., "Biochars derived from bamboo and rice straw for sorption of basic red dyes," *PLOS ONE*, vol. 16(7), pp. e0254637, 2021.

Smith, A.T., LaChance, A. M., Zeng, S., Liu, B., and Sun, L., "Synthesis, properties, and applications of graphene oxide/reduced graphene oxide and their nanocomposites," *Nano Materials Science*, vol. 1(1), pp. 31-47, 2019.

Suhan, M.B.K, Shuchi, S. B., Anis, A., Haque, Z., and Islam, M. S., "Comparative degradation study of remazol black B dye using electro-coagulation and electro-Fenton process: Kinetics and cost analysis," *Environmental Nanotechnology, Monitoring & Management*, vol. 14, pp. 100335, 2020.

Suhan, M. B. K., Mahtab, S. T., Aziz, W., Akter, S., and Islam, M. S., "Sudan black B dye degradation in aqueous solution by Fenton oxidation process: Kinetics and cost analysis," *Case Studies in Chemical and Environmental Engineering*, vol. 4, 2021.

Sun, B., Yuan, Y., Li, H., Li, X., Zhang, C., Guo, F., Liu, X., Wang, K., and Zhao, X., "Waste-cellulose-derived porous carbon adsorbents for methyl orange removal," *Chemical Engineering Journal*, vol. 371, pp. 55–63, 2019.

Tan, X. F., Liu, Y. G., Gu, Y. L., Xu, Y., Zeng, G. M., Hu, X. J., and Li, J., "Biochar-based nanocomposites for the decontamination of wastewater: A review," *Bioresource technology*, vol. 212, pp. 318-333, 2016.

Torres-Cruz, N., Rivero-Angeles, M. E., Rubino, G., Menchaca-Mendez, R., Menchaca-Mendez, R., and Ramirez, D., "A comprehensive analytical framework for VoD services in hybrid CDN-P2P systems," *Journal of Network and Computer Applications*, vol. 161, pp. 102643, 2020.

Tsamo, C., Assabe, M., Argue, J., and Ihimbru, S., "Discoloration of methylene blue and slaughterhouse wastewater using maize cob biochar produced using a constructed burning chamber: A comparative study," *Scientific African*, vol. 3, pp. e00078, 2019.

Varma, R., and Vasudevan, S., "Extraction, Characterization, and Antimicrobial Activity of Chitosan from Horse Mussel *Modiolus modiolus*," *ACS Omega*, vol. 5(32), pp. 20224–20230, 2020.

Virtanen, T., Rudolph, G., Lopatina, A., Al-Rudainy, B., Schagerlöf, H., Puro, L., Kallioinen, M., and Lipnizki, F., “Analysis of membrane fouling by Brunauer-Emmet-Teller nitrogen adsorption/desorption technique,” *Scientific Reports*, vol. 10(1), 2020.

Wadhawan, S., Jain, A., Nayyar, J., and Mehta, S. K., “Role of nanomaterials as adsorbents in heavy metal ion removal from wastewater: A review,” *Journal of Water Process Engineering*, vol. 33, pp. 101038, 2020.

Wang, L., Wang, Y., Ma, F., Tankpa, V., Bai, S., Guo, X., and Wang, X., “Mechanisms and reutilization of modified biochar used for removal of heavy metals from wastewater: A review,” *Science of The Total Environment*, vol. 668, pp. 1298-1309, 2019.

Wang, X., Guo, Z., Hu, Z., and Zhang, J., “Recent advances in biochar application for water and wastewater treatment: a review,” *Peer Journal*, vol. 8, pp. e9164, 2020.

Wang, S., Ai, S., Nzediegwu, C., Kwak, J.H., Islam, M.S., Li, Y., and Chang S.X., “Carboxyl and hydroxyl groups enhance ammonium adsorption capacity of iron (III) chloride and hydrochloric acid modified biochars,” *Bioresource Technology*, vol. 309, pp. 123390, 2020.

Wang, S., Kwak, J.H., Islam, M. S., Naeth, M. A., El-Din, M. G., and Chang, S X., “Biochar surface complexation and Ni (II), Cu (II), and Cd (II) adsorption in aqueous solutions depend on feedstock type,” *Science of The Total Environment*, vol. 712, pp. 136538, 2020.

Wesley, M. J., Lerner, R. N., Kim, E-S, Islam, M. S., and Liu, Y., “Biological fixed film,” *Water Environment Research*, Vol. 83(10), pp. 1150-1186, 2011.

Wong, S., Ghafar, N. A., Ngadi, N., Razmi, F. A., Inuwa, I. M., Mat, R., and Amin, N. A. S., “Effective removal of anionic textile dyes using adsorbent synthesized from coffee waste,” *Scientific Reports*, vol. 10(1), 2020.

Wu, M., Feng, Q., Sun, X., Wang, H., Gielen, G., and Wu, W., “Rice (*Oryza sativa* L) plantation affects the stability of biochar in paddy soil,” *Scientific Reports*, vol. 5(1), 2015.

Xiang, W., Zhang, X., Chen, J., Zou, W., He, F., Hu, X., and Gao, B., “Biochar technology in wastewater treatment: A critical review.” *Chemosphere*, vol. 252, pp. 126539, 2020.

Yang, C., Xu, W., Nan, Y., Wang, Y., Hu, Y., Gao, C., and Chen, X., “Fabrication and characterization of a high performance polyimide ultrafiltration membrane for dye removal,” *Journal of colloid and interface science*, vol. 562, pp. 589-597, 2020.

Yaseen, D. A., and Scholz, M., "Textile dye wastewater characteristics and constituents of synthetic effluents: a critical review," *International journal of environmental science and technology*, vol. 16(2), pp. 1193-1226, 2019.

Yaashikaa, P.R., Kumar, P. S., Varjani, S., and Saravana, A., "A critical review on the biochar production techniques, characterization, stability and applications for circular bioeconomy," *Biotechnology Reports*, vol. 28, pp. e00570, 2020.

Yao, X., Ji, L., Guo, J., Ge, S., Lu, W., Chen, Y., Cai, L., Wang, Y., and Song, W., "An abundant porous biochar material derived from wakame (*Undaria pinnatifida*) with high adsorption performance for three organic dyes," *Bioresource Technology*, vol. 318, pp. 124082, 2020.

Yogalakshmi, K. N., Das, A., Rani, G., Jaswal, V., and Randhawa, J. S., "Nano-bioremediation: a new age technology for the treatment of dyes in textile effluents," In *Bioremediation of Industrial Waste for Environmental Safety*, pp. 313-347, 2020.

Yusuf, M., "Synthetic Dyes: A Threat to the Environment and Water Ecosystem," *Textiles and Clothing*, pp. 11-26, 2019.

Yu, L., Xi, J., Li, M., Chan, H., Su, T., Phillips, D., and Chan, W., "The degradation mechanism of methyl orange under photo-catalysis of TiO₂," *Physical Chemistry Chemical Physics*, vol. 14(10), pp. 3589-3595, 2012.

Zafar, M. N., Dar, Q., Nawaz, F., Zafar, M. N., Iqbal, M., and Nazar, M. F., "Effective adsorptive removal of azo dyes over spherical ZnO nanoparticles," *Journal of Materials Research and Technology*, vol. 8(1), pp. 713–725, 2019.

Zaharia, C., Suteu, D., Muresan, A., and Popescu, A., "Textile wastewater treatment by homogeneous oxidation with hydrogen peroxide," *Environmental engineering and management journal*, vol. 8, pp. 1359-1369, 2009.

Zaini, M. A. A., Zakaria, M., Alias, N., Zakaria, Z. Y., Johari, A., Setapar, S. H. M., Kamaruddin, M. J., and Yunus, M. A. C., "Removal of Heavy Metals onto KOH-activated Ash-rich Sludge Adsorbent," *Energy Procedia*, vol. 61, pp. 2572–2575, 2014.

Zamri, N. I. I., Zulmajdi, S. L. N., Daud, N. Z. A., Mahadi, A. H., Kusrini, E., and Usman, A., "Insight into the adsorption kinetics, mechanism, and thermodynamics of methylene blue from aqueous solution onto pectin-alginate-titania composite microparticles," *SN Applied Sciences*, vol. 3(2), 2021.

Zhang, Y., Islam, M. S., Dong, S. McPhedran, K. N., Rashed, E. M., El-Shafei, M. M., Nouredin, A. M., and Gamal El-Din, M., A., “Comparative Study of microbial dynamics and phosphorus removal for two innovative side-stream wastewater treatment processes,” *RSC Advances*, vol. 7, pp. 45938-45948, 2017.

Zhao, T., Ma, X., Cai, H., Ma, Z., and Liang, H., “Study on the Adsorption of CuFe₂O₄-Loaded Corncob Biochar for Pb(II),” *Molecules*, vol. 25(15), pp. 3456, 2020.

Zhou, Y., Gao, B., Zimmerman, A. R., Fang, J., Sun, Y., and Cao, X., “Sorption of heavy metals on chitosan-modified biochars and its biological effects,” *Chemical Engineering Journal*, vol. 231, pp. 512–518, 2013.

Zhu, H. Y., Jiang, R., and Xiao, L., “Adsorption of an anionic azo dye by chitosan/kaolin/ γ -Fe₂O₃ composites,” *Applied Clay Science*, vol. 48(3), pp. 522–526, 2010.